Anatomical Basis of Sun Compass Navigation II: The Neuronal Composition of the Central Complex of the Monarch Butterfly

Stanley Heinze,[1]* Jeremy Florman,[1] Surainder Asokaraj,[1] Basil el Jundi,[2] and Steven M. Reppert[1]*

[1]Department of Neurobiology, University of Massachusetts Medical School, Worcester, Massachusetts 01605
[2]Department of Biology, University of Lund, 22362 Lund, Sweden

ABSTRACT

Each fall, eastern North American monarch butterflies in their northern range undergo a long-distance migration south to their overwintering grounds in Mexico. Migrants use a time-compensated sun compass to determine directionality during the migration. This compass system uses information extracted from sun-derived skylight cues that is compensated for time of day and ultimately transformed into the appropriate motor commands. The central complex (CX) is likely the site of the actual sun compass, because neurons in this brain region are tuned to specific skylight cues. To help illuminate the neural basis of sun compass navigation, we examined the neuronal composition of the CX and its associated brain regions. We generated a standardized version of the *sun compass neuropils*, providing reference volumes, as well as a common frame of reference for the registration of neuron morphologies. Volumetric comparisons between migratory and nonmigratory monarchs substantiated the proposed involvement of the CX and related brain areas in migratory behavior. Through registration of more than 55 neurons of 34 cell types, we were able to delineate the major input pathways to the CX, output pathways, and intrinsic neurons. Comparison of these neural elements with those of other species, especially the desert locust, revealed a surprising degree of conservation. From these interspecies data, we have established key components of a conserved core network of the CX, likely complemented by species-specific neurons, which together may comprise the neural substrates underlying the computations performed by the CX. J. Comp. Neurol. 521:267–298, 2013.

INDEXING TERMS: central complex; anterior optic tubercle; neuropil volumes; visual system; *Danaus plexippus*; comparative neuroanatomy

Each fall, millions of eastern North American monarch butterflies (*Danaus plexippus*) undergo a long-distance migration from the northern United States and southern Canada to their overwintering grounds in central Mexico. Behavioral experiments have revealed that a time-compensated sun compass allows migrants to perceive sky compass cues, integrate them with the current time of day, and generate the appropriate southerly flight vector (Reppert et al., 2010). Electrophysiological work has shown that neurons of the monarch butterfly's central brain respond to skylight cues (Heinze and Reppert, 2011), whereas molecular and behavioral work has shown that the antennae house the internal clocks required for time compensation (Merlin et al., 2009). These findings, along with anatomical links between brain clocks and the proposed compass-related brain regions (Sauman et al., 2005; Zhu et al., 2008), suggest that a complex neuronal network in the monarch brain integrates time and compass information to generate appropriate motor commands.

At the center of this sun compass network is the central complex (CX), a group of neuropils consisting of the protocerebral bridge (PB), the upper and lower division of

Additional Supporting Information may be found in the online version of this article.

Grant sponsor: Air Force Office of Scientific Research; Grant number: FA9550-10-1-0480; Grant sponsor: the Human Frontier Science Program; Long-term fellowship number: LT000379/2009-L (to S.H.).

*CORRESPONDENCE TO: Stanley Heinze, University of Massachusetts Medical School, Department of Neurobiology, 364 Plantation Street, Worcester, MA, 01605. E-mail: stanley.heinze@umassmed.edu; or Steven Reppert, University of Massachusetts Medical School, Department of Neurobiology, 364 Plantation Street, Worcester, MA, 01605. E-mail: steven.reppert@umassmed.edu

Received July 13, 2012; Revised August 1, 2012; Accepted August 3, 2012
DOI 10.1002/cne.23214
Published online August 8, 2012 in Wiley Online Library (wileyonlinelibrary.com)

the central body (CBU, CBL), and the paired noduli. This highly conserved brain region contains an internal representation of azimuthal space in the desert locust (*Schistocerca gregaria*), and likely serves as an internal sun compass in migratory monarchs as well (Heinze and Homberg, 2007). Additionally, work in other species, in particular flies and cockroaches, suggests that the CX also possesses functions in spatial memory (Neuser et al., 2008), visual learning (Liu et al., 2006), multimodal integration (Homberg, 1994; Ritzmann et al., 2008), and motor control (Strauss, 2002; Bender et al., 2010; Triphan et al., 2010). Whether these diverse functions are restricted to different species or are all individual aspects of an underlying, global function common to insects remains to be determined. Comparing the detailed neuronal layout of the CX among diverse species will help resolve this issue.

In all insect species examined, the CX has been shown to possess a highly regular neuroarchitecture, composed of vertical columns (in the PB and central body) and horizontal layers (in the central body) (Williams, 1975; Strausfeld, 1999; Heinze and Homberg, 2008; Homberg, 2008). Golgi studies and single-cell dye injections have revealed that three major classes of neurons produce this stereotypical layout: 1) tangential neurons connect diverse regions of the brain to entire layers of one of the CX components; 2) columnar neurons connect single columns of the PB and/or the central body to either the noduli, the lateral accessory lobes (LAL), or (in locusts) the anterior lip; and 3) pontine neurons provide interhemispheric connections between two individual columns of the CBU (Homberg, 1985; Hanesch et al., 1989; M̈ller et al., 1997; Heinze and Homberg, 2008). Detailed catalogues of neuronal elements comprising the CX exist for *Drosophila melanogaster* (Hanesch et al., 1989) and for the desert locust (Heinze and Homberg, 2008), whereas information about other insect species, including the monarch butterfly (Heinze and Reppert, 2011), remains fragmentary. In all species, the LALs are intricately connected with the CX, and electrophysiological and anatomical studies propose a major role for these neuropils in the processing of polarized light (a major skylight compass cue) across insects (Vitzhum et al., 2002; Homberg et al., 2003, 2011; Heinze and Reppert, 2011; Pfeiffer and Kinoshita, 2012). These studies also place the anterior optic tubercle (AOTu) directly upstream of the LAL. Collectively, the CX, LAL, and AOTu are an interconnected and functionally related group of brain regions, which, in the monarch, we refer to as *sun compass neuropils*. The detailed layout of compass neuropils has been recently described for the monarch by 3D reconstructions and immunocytochemical staining (Heinze and Reppert, 2012). However, only a very few neurons have been reported that occupy these neuropils (Heinze and Reppert, 2011).

To directly compare neurons visualized in different individuals in the current study, we created a standardized, average-shape representation of sun compass neuropils for the monarch brain. The volumetric data provided by the standardized compass neuropils was used as a reference to identify changes in brain structure correlating with the different behavioral states of the monarch (e.g., nonmigratory versus migratory). We also used the standard to register 3D reconstructions of individual neurons to generate a comprehensive neuronal catalogue, identifying numerous neuronal types intrinsic to the CX, as well as outlining proposed input and output pathways to and from the CX. These reconstructions form the foundation of a comprehensive 3D database of the neuronal composition of the monarch butterfly sun compass.

Abbreviations

AOTu	anterior optic tubercle
aLobl	anterior loblet
CBL	lower division of the central body
CBU	upper division of the central body
dLAL	dorsal LAL
LAL	lateral accessory lobe
LT	lateral triangle
LU	lower unit
MB-Lb	mushroom body lobes
No	noduli
NU	nodular unit
PB	protocerebral bridge
SP	strap
UU	upper unit
vLAL	ventral LAL

MATERIALS AND METHODS

Animals

Different sources of eastern North American monarch butterflies were used for different study aspects. For standardization of the compass neuropils, the male offspring of nonmigratory butterflies reared outdoors near Greenfield, Massachusetts were used. These animals were brought to the laboratory as pupae (August, 2010), and the adults emerged in environmentally controlled incubators (lighting, 12-hour light:12-hour dark; humidity, 70%; temperature, 25°C). After adult eclosion, butterflies were kept in glassine envelopes for 30–40 days. They were fed every other day with a 25% honey solution.

For volumetric comparison with the reference volumes provided by the standardized compass neuropils, we used four different groups of animals. Summer (nonmigratory) monarchs (four males and four females) were netted near Greenfield, Massachusetts in early August 2011. These animals were kept for 7 days in the laboratory (under the conditions described above) before dissection. Migratory monarchs from Texas were collected from roosts or netted during daytime flight and shipped to the

TABLE 1.
Primary Antibodies Used in This Study

Antigen	Immunogen	Manufacturer, species, type, cat. no.	Dilution
Synapsin	Fusion protein of glutathione-S-transferase and the *Drosophila* SYN1 protein	Developed by G. Buchner (University of Würzburg, Germany), obtained from the Developmental Studies Hybridoma Bank, University of Iowa; mouse, monoclonal, 3C11	1:50
Serotonin	Serotonin coupled to bovine serum albumin (BSA) with paraformaldehyde	Immunostar, rabbit, polyclonal, 20080, lot 5420201	1:4,000

laboratory; their brains were dissected after arrival. To balance out possible differences between individual migrant populations, animals were collected in two consecutive years (four males, one female from October/November 2010, Eagle Pass, Texas/Port Lavaca, Texas; five males from October 2011, Port Lavaca, Texas). For control experiments, Massachusetts migrants were netted near Greenfield in late September, and five males were dissected after capture. Aged Massachusetts migrants were produced by keeping some of the Greenfield-collected migrants in glassine envelopes under fall conditions (lighting, 11-hour light:13-hour dark; humidity, 70%; temperature, 23°C in light and 12°C in dark) for 2 months before dissection; only male animals were used. The migratory status of the migrant butterflies was confirmed by behavioral experiments in a flight simulator (P.A. Guerra, S.M. Reppert, unpublished data).

Neurobiotin injections were performed mainly on wild-caught animals of both sexes (migrants from Texas or Florida; nonmigrants from Massachusetts). Some butterflies were obtained from a commercial breeder (Shady Oak Butterfly Farm, Brooker, FL). During the migratory season, all butterflies kept in the laboratory were maintained under fall-like conditions, whereas during the summer months, animals were maintained under laboratory conditions (lighting, 12-hour light:12-hour dark; humidity, 70%; temperature, 25°C).

Neurobiotin injections and histology

Neurons were iontophoretically injected with neurobiotin during intracellular recordings (for details, see Heinze and Reppert, 2011). In brief, animals were fixed with wax on a metal holder, the head capsule was opened, the neural sheath was removed, and the recording electrode was inserted into the brain (resistance 80–140 MΩ). Electrode tips were filled with 4% Neurobiotin (Vector, Burlingame, CA; in 1 M KCl) and topped off with 1 M KCl. Depolarizing current (0.5–3 nA) was continuously applied for up to 3 minutes when the electrode was positioned inside a neurite. Alternatively, mass stainings were achieved with the electrode positioned near neurons with the application of 40 nA of pulsed current (1 Hz, for 30 minutes).

After injection, brains were dissected out of the head capsule in Ringer's solution (150 mM NaCl, 3 mM KCl, 10 mM N-tris[hydroxymethyl]-methyl-2-aminoethane-sulfonic acid [TES], 25 mM sucrose, 3 mM $CaCl_2$; pH 6.9; King et al., 2000), fixed in Neurobiotin fixative (4% paraformaldehyde [PFA], 2% saturated picric acid, 0.25% glutaraldehyde, in 0.1 M phosphate buffer, pH 7.4) overnight at 4°C. Brains were rinsed in phosphate buffer (4 × 15 minutes) and incubated with Cy3-conjugated streptavidin (Rockland, Boyertown, PA; 1:1,000, in 0.1 M phosphate-buffered saline (PBS) with 0.3% Triton X-100, 4°C) for 3 days. Next, the brains were rinsed in PBS (4 × 20 minutes) and PBT (PBS with 0.3% Triton X-100; 2 × 20 minutes) and dehydrated in an increasing ethanol series (25%, 50%, 70%, 90%, 95%, 100%, 15 minutes each). The brains were transferred into a fresh mixture of methyl salicylate and ethanol (1:1; 15 minutes), in which the ethanol was allowed to evaporate to ensure a smooth transition to pure methyl salicylate. Finally, the brains were cleared for 35 minutes in pure methyl salicylate and embedded in Permount (Fisher Scientific, Fair Lawn, NJ) between two coverslips. Plastic reinforcing rings were used as spacers to avoid squeezing.

Antibodies

The anti-synapsin antibody was a monoclonal antibody raised in mouse against fusion proteins consisting of glutathione-S-transferase and the *Drosophila* SYN1 protein (SYNORF1; Table 1; Klagges et al., 1996). Its specificity has been characterized by Klagges et al. (1996). It has been shown to label synaptic neuropil in a wide range of species (e.g., Brandt et al., 2005; Kurylas et al., 2008; el Jundi et al., 2009; Dreyer et al., 2010), including monarch butterflies (Heinze and Reppert, 2011, 2012).

The anti-5HT (serotonin) antiserum (polyclonal, raised in rabbit; Table 1) exhibits no cross-reactivity to 5-hydroxytryptophan, 5-hydroxyindole, 5-hydroxy-indole-3-acetic acid, or dopamine in Bn-SA/horseradish peroxidase (HRP) labeling assays (Immunostar, Hudson, WI; histochemical serotonin antisera specification sheet). The specificity of the anti-5HT antiserum on monarch brain sections was tested by preadsorption of the diluted antiserum with different concentrations of 5HT-BSA conjugate (Immunostar). At a concentration of 20 μg/ml all staining was abolished, whereas faint residual staining

was present at lower concentrations (Heinze and Reppert, 2012).

Immunolabeling of wholemount preparations

Before dissection, the animals were cooled on ice, decapitated, mounted in small wax dishes, and covered in ice-cold HEPES-buffered saline (HBS; 150 mM NaCl; 5 mM KCl; 5 mM $CaCl_2$; 25 mM sucrose; 10 mM HEPES (N-[2-hydroxyethyl]piperazine-N′-[2-ethanesulphonic acid]); pH 7.4; Ott, 2008). The brains were dissected from the head capsule within 10 minutes and transferred into the fixative (0.25% [18.4 mM] $ZnCl_2$, 135 mM NaCl, 35 mM sucrose, 1% PFA; Ott, 2008). After the brain was freed of trachea and fatbody, the retina was carefully removed. Fixation lasted for 20 hours at room temperature. The brains were then washed in HBS (8 × 25 minutes), permeabilized by incubation in a mixture of methanol and dimethylsulfoxide (DMSO; ratio 20:80, 75 minutes), and rinsed in 0.1 M Tris buffer (3 × 10 minutes; pH 7.5) at room temperature. Preincubation was performed with 5% normal goat serum (NGS; in 0.1 M PBT) overnight at 4°C. The primary antibody (anti-synapsin) was applied for 5 days at 4°C (with 1% NGS in 0.1 M PBT). The brains were intensely rinsed (8 × 25 minutes in PBT), before incubation with the secondary antibody (3 days at 4°C; DyLight647-conjugated goat anti-mouse, 1:300; with 1% NGS in 0.1 M PBT; Jackson ImmunoResearch, West Grove, PA). After more washing steps (6 × 25 minutes in 0.1 M PBT, 2 × 25 minutes in 0.1 M PBS), the brains were dehydrated, cleared, and mounted as described for Neurobiotin-injected brains.

Immunolabeling of rehydrated thick sections

To evaluate neuron morphologies in detail, we performed high-resolution confocal microscopy of Neurobiotin-injected neurons combined with immunocytochemical labeling. Because the working distance of high-magnification objectives is limited, these analyses could not be done in wholemount preparations. Therefore, we selected Neurobiotin-injected preparations containing neurons of interest that had already been scanned at lower resolution. These mounted brains were incubated in Xylene until all mounting medium (Permount) was dissolved (2–3 hours) and subsequently rehydrated in a decreasing ethanol series (100%, 95%, 90%, 70%, 50%, 25%; 15 minutes each). After the brains were rinsed in PBS (3 × 15 minutes), they were embedded in albumin–gelatin (4.8% gelatin and 12% ovalbumin in demineralized water), postfixed overnight in 4% formalin solution at 4°C, and cut into 120-μm-thick sections with a vibrating blade microtome (Leica VT1200).

After washing in 0.1 M PBS (3 × 15 minutes), the sections were treated identically to wholemount preparations, but with reduced incubation times, as follows. Preincubation (5% NGS/NDS, in 0.1 M PBT) was for 3 hours at room temperature. Primary antibody incubation (anti-synapsin, anti-serotonin, in 0.1 M PBT with 1% NGS/NDS) was for 4 days at 4°C. Secondary antibody incubation (DyLight648-conjugated goat-anti-mouse [Jackson ImmunoResearch; 1:300]; DyLight488-conjugated donkey-anti-rabbit [Jackson ImmunoResearch; 1:300], in 0.1 M PBT with 1% NGS/NDS) was for 2 days at 4°C. Between both antibody incubations, sections were rinsed with PBT (6 × 15 minutes). To refresh Neurobiotin labeling, Cy3-conjugated streptavidin (1:1,000) was added to both antibody incubations. After washing with PBT (4 × 15 minutes) and PBS (2 × 15 minutes), the sections were dehydrated in an increasing ethanol series (10 minutes for each step) and cleared in methyl salicylate (20 minutes). The sections were embedded in Permount between two coverslips with appropriate spacers.

Image acquisition and processing

All images were acquired by using confocal microscopy (most images: Zeiss LSM 5 Pascal). For 3D reconstructions of neuropils and neurons, wholemount preparations were imaged with a 25× objective (LD LCI Plan-Apochromat 25×/0.8 Imm Corr DIC; Zeiss). To cover the full extent of all sun compass neuropils, six overlapping image stacks had to be acquired (four image stacks from anterior and two from posterior), which were subsequently aligned and merged by using either the ImageJ implementation FIJI (general public license, downloadable from http://fiji.sc) or Amira5.2 (Mercury Computer Systems, San Diego, CA). Finally, all neuropil scans were resampled to a voxel size of 1 μm^3. Imaging of thick sections was done either at 25× (see above) or with a 40× objective (EC Plan-Neofluar 40x/1.3 Oil DIC, Zeiss; at Zeiss LSM 700) for all high-resolution images (voxel size: 0.1 × 0.1 × 0.3 μm). Most images were optimized for brightness and contrast and are displayed as maximal intensity projections.

3D reconstructions

All neuropil reconstructions were based on anti-synapsin–labeled wholemount preparations and were performed in Amira5.2, as described in detail in Heinze and Reppert (2012). In short, confocal image stacks containing the compass neuropils were aligned, merged, and resampled. From the resulting image stack a label field was created, in which voxels were assigned to individual neuropils. After completion of the label field, a polygonal surface model was automatically calculated. The color code for the compass neuropils was according to Heinze and Reppert (2012).

For tracing neuron morphologies, we used the skeletonize plugin for Amira5.2 (Schmitt et al., 2004). Before reconstructions, confocal image stacks containing the neuron were aligned into a consistent frame of reference. Based on these image stacks, a skeleton tree was created by manually tracing all neurites of a cell and applying a fitting algorithm that adjusted midline and diameter of each neuronal segment according to local image data. For reconstructions based on wholemount preparations (25× objective), this fitted skeleton tree was the final result of the reconstruction. Different color maps were applied to visualize quantitative features of the skeleton tree (e.g., distance of segments along the neurite from the origin of the tree). It should be noted that very dense, small arborization trees could not always be fully resolved from the confocal images. In these cases, the space occupied by the arborizations was semirandomly filled with fibers to account for the extent and location of the arborization tree with respect to surrounding neuropils. Consequently, the internal fine-structure of these arborization trees was not preserved in the reconstruction.

To obtain realistic representations of the surface of a neuron, some skeleton trees based on high-resolution data (40× objective) were processed further. The skeletonize tool was used to create a triangulated surface reconstruction of the cell by combining information from the skeleton tree (diameter, midline) with local image data (Schmitt et al., 2004; Evers et al., 2005). Different color maps could be applied to visualize regions of the neuron overlapping with antibody labeling or label fields.

Standardization of compass neuropils

For the standardization process, we reconstructed the compass neuropils of 10 male, laboratory-raised monarch butterflies (details given above) and applied the iterative shape averaging (ISA) protocol to the data obtained from the anti-synapsin–labeled brains (Brandt et al., 2005). Five confocal image stacks were scanned from each brain, merged into a single file, and resampled to a final voxel size of 1 μm^3. For each brain, these image stacks were used to generate a label field (see above).

As the ISA protocol utilizes the gray values of the image data to extract contrast information (edges, etc.), artificial edges created by the boundaries of the image stacks had to be eliminated. We thus eliminated all image data from regions of the image stacks further than 10 voxels away from the reconstructed neuropil surfaces, by using the Arithmetic tool of Amira. The resulting "cut-out" image stack was subjected to the ISA protocol (according to el Jundi et al., 2010).

The details of the ISA protocol have been described previously (Brandt et al., 2005; Kurylas et al., 2008; el Jundi et al., 2010; Wei et al., 2010) and will thus only be broadly outlined here. First, a template brain was selected, which subsequently served as a reference to register all remaining brains. As this brain influences the final neuropil volumes of the ISA standard, we calculated the mean neuropil volumes from all 10 brains, and chose the individual brain as template that possessed the volumes closest to the population average. During the first round of registration, all original image stacks were globally registered onto the template brain by using an affine (9 degrees of freedom) registration. This step compensates the position, rotation, and global size between individual image stacks. In a second round, to correct shape differences between individual brains, nonrigid deformation (elastic) transformations were applied iteratively to the image stacks. For this purpose, the resulting average brain of the affine registration was used as a template for the elastic registration. The elastic registration was repeated four times, with the previous result being used as the template for each subsequent run. The final result was an average image stack.

The transformation parameters obtained from all registrations were then applied to the corresponding 10 original label fields, thus generating an average, standardized surface reconstruction of the monarch compass neuropils. This average label field represents the most important result of the standardization process. It should be noted that the volumes of the standardized neuropils are not average volumes but depend on the selected template brain. Average volumes were thus calculated based on the 10 original label fields. All computations in the context of the ISA protocol were performed on a Linux cluster based at the HRZ-Marburg.

Registration of neurons onto standardized neuropils

To register individual neurons from different animals onto a common frame of reference, we reconstructed the neuropils innervated by each neuron based on background staining directly from individual wholemount preparations. The only structures not reliably recognizable from background fluorescence were the small subunits of the AOTu. Therefore, all reconstructions of TuLAL and TuTu neurons were based on rehydrated, anti-synapsin–labeled preparations (thick sections). For neuropil reconstruction, the image stacks containing the neuron were merged and resampled to the same voxel size as the standard (1 μm^3). After generation of the label field of the innervated neuropils, their respective counterparts in the standard were isolated. In a first registration step, an affine transformation was performed to match the position, orientation, and size of the individual neuropils to their standardized counterparts (parameters: translation, rotation, anisometric scaling). The transformation parameters obtained were then applied to the reconstructed

skeleton tree. Before performing the second step, the elastic registration, we down-sampled the label fields resulting from the affine registration twofold, which substantially reduced processing time with the given computational capabilities. The elastic registration was performed with five iterations and resulted in the generation of a vector field that defined the transformations at each voxel of the data stack. This vector field was used to apply the transformations obtained from the neuropil registration to the reconstructed skeleton tree (result of the affine registration). The transformed skeleton tree was the final result of the registration process. All manipulations were performed in Amira5.2.

Limitations of the registration process

The registration method used for neurons is a tradeoff between optimal quality and workload, so that several sources of imprecision have to be addressed. First, no inferences about fiber location can be drawn below the voxel size of 2 μm^3. Second, as reconstructions of neuropils in which individual neurons arborize were based on background fluorescence, they might not be 100% identical to reconstructions based on anti-synapsin labeling. We addressed this problem by comparing neuropils reconstructed from background fluorescence with reconstructions of the identical neuropil after rehydration and anti-synapsin labeling. No major differences were obvious in the examples examined that could be assigned to misinterpretation of background fluorescence. On the contrary, because anti-synapsin counterstaining can only be performed on rehydrated thick sections (Heinze and Homberg, 2008; el Jundi et al., 2010), our new approach overcomes considerable complications. Imaging directly from whole-mount preparations does not require sectioning and re-/dehydration, processes that otherwise produce shrinkage artifacts and tissue loss (at the cutting edges) and thus lead to uncertainties in section alignment and errors in the final neuropil shape (el Jundi et al., 2010).

Because of the large number of neurons we registered into the standard, we were able to identify some limitations of the registration process more clearly than in previous uses of this method (Brandt et al, 2005; el Jundi et al., 2010; Løfaldli et al., 2010). The highest precision in the registration process was observed close to surfaces of highly defined neuropils with low interindividual variability. The least reliable results can be expected for innervations of the unstructured protocerebrum. As no standardized landmarks are present close to some of these fibers, the registration process is largely restricted to the affine registration. Thus, only the broad size and orientation are standardized, but no local differences of the individual brains are corrected. Furthermore, regions with high variability in their relative position, particularly the PB, are occasionally matched imprecisely during affine registration, if good overlap of the original structure with the standard cannot be generated. This leads to more pronounced elastic deformations, misplacing the centers of ramifications by up to 10% along the length of the PB in some cases (when compared with their position in the original brain). At last, some neuropils, in particular the LAL, are comparably poorly defined structures, that is, they show high variability in shape, as well as some ambiguous boundaries. This leads to some uncertainty in the final position of fibers near these poorly defined neuropil boundaries (e.g., within the isthmus tracts or near the posterior LAL boundary), as well as to occasional overstretching of individual branches and sudden jumps in neurite paths.

Nomenclature of cell types

In general, the names used for monarch neurons were adopted from the those of the desert locust, as compass-related neurons have been best studies in this species (Müller et al., 1997; Heinze and Homberg, 2008). Moreover, the locust nomenclature scheme is systematically organized and new cell types can be added easily. As homologous monarch neurons may not exist for some locust cell types, gaps in the nomenclature (e.g., lack of CPU3 cells in the monarch) will not necessarily be filled by additional types of neuron in the future.

No system for nomenclature of CBU tangential neurons exists in the locust. Furthermore, it did not seem useful to adapt the naming system for fan-shaped neurons in *Drosophila* for the monarch, as the distinction between FI and Fm neurons (Hanesch et al., 1989; Young and Armstrong, 2010) is based on the path of the fiber entering the fan-shaped body (CBU) either from the side or through the center of the ellipsoid body (CBL). Due to the different shape of the CBL in monarchs and flies, defining homologous cell types is problematic. Therefore, a new nomenclature system for CBU tangential cells was developed that built on the locust naming system for tangential cells of the CBL. To cover the complexity of this class of neurons, the locations of the somata, as well as the innervated CBU layers, were used to encode the neuron type. This has several advantages. First, a grouping of neurons according to the location of their somata likely combines cells of similar developmental origin. Second, the descriptive and systematic nature of the scheme allows easy additions of new cell types. Finally, no reference to unstructured regions of the protocerebrum is made in the neuron names, as these are divergent between species, and boundaries can potentially change over time with new functional insights. Thus, the new scheme can be easily adopted for other species, and interspecies comparisons will be facilitated.

Volumetric analysis

Data on neuropil volumes were extracted from the label fields of individual brains by means of the TissueStatistics tool in Amira. After verifying that no significant difference occurred between the right and left counterparts of any neuropil (Student's *t*-test; not shown), we summed the volumes of corresponding neuropils of both brain hemispheres. This simplified subsequent analysis and eliminated intrahemispheric variability. All statistical analysis was performed in GraphPad (San Diego, CA) Prism5 (α value: 0.05 for all tests).

For display of absolute volume data, we calculated means and standard deviations of each neuropil in all five groups of butterflies. These values were subtracted from the corresponding reference volumes to visualize the absolute deviations from the standardized compass neuropils. To test whether these differences were statistically significant, we subjected the original raw data to one-way analysis of variance (ANOVA). In this way, each neuropil was compared separately between the five groups of monarchs. Post hoc comparison (Bonferroni test) was done for the comparisons graphically displayed (standard versus all others, Massachusetts-old versus Massachusetts-young). For neuropils, in which at least one group differed significantly from normal distribution (tested with the Kolmogorov–Smirnov test with Lilliefors' correction), we used the nonparametric ANOVA equivalent (Kruskal–Wallis test, with Dunn's post hoc test).

Relative volumes were calculated by normalizing each neuropil volume by the total volumes of all combined compass neuropils of that particular brain. Display of deviations from the standardized compass neuropils and statistical analysis were performed as for absolute volume data. Additionally, the relative volume of the PB was compared across all migratory animals with one-way ANOVA combined with the Bonferroni post hoc test (all possible comparisons, three groups).

Allometric relations of neuropils were analyzed by linear regression of absolute volumes of each neuropil against the combined volumes of all remaining components of the compass neuropils (according to Ott and Rogers, 2010). An F-test was used to test whether the slope of the regression line was significantly different from zero. Slopes and intercepts of multiple regression lines were compared by analysis of covariance (ANCOVA).

RESULTS

Standardized average-shape sun compass neuropils

The main purpose of the current work was to provide a detailed description of the major neurons within the sun compass neuropils of the monarch brain (see below). However, because of interindividual variability, neurons reconstructed from different butterflies cannot be compared easily, and predictions about common projection areas are error prone. To overcome these obstacles, we generated a standardized, average-shape representation of the monarch compass neuropils. For this purpose, we used 10 male, laboratory-raised monarch butterflies, maintained in glassine envelopes for 1 month after eclosion. These animals were chosen to obtain a "default" state of the monarch butterfly brain, that is, animals not having had migratory or foraging experience in the wild, while still allowing age-related neural processes to occur.

The chosen method for standardization was the ISA protocol previously used for the honey bee brain (Brandt et al., 2005), the desert locust brain (Kurylas et al., 2008), the brain of the moth *Heliothis virescens* (Kvello et al., 2009), and the brain of the cockroach *Leucophaea maderae* (Wei et al., 2010), as well as the CX of the desert locust (el Jundi et al., 2010). This procedure preserves the relative location and shape of neuropils and is thus well suited as a common frame of reference for the registration of single neurons (Kurylas et al., 2008; el Jundi et al., 2010).

Overall, 10 neuropils (eight paired and two unpaired) were included in the standard (Fig. 1): the CBU, CBL, PB, and noduli of the CX; the lateral triangle (LT) and the LAL proper of the LAL; and the upper unit, lower unit, nodular unit, and strap of the AOTu. It should be noted that, unlike in most insects, the PB of the monarch is not a continuous structure across the midline, and it was thus counted as a paired neuropil. The neuropil reconstructions were based on anti-synapsin labeling, and the boundaries of regions were used as defined by Heinze and Reppert (2012).

The standardized sun compass neuropils as a volumetric reference

The standardized sun compass neuropils provide a set of reference volumes for these brain regions (Fig. 1E,F, Table 2). Because animals without any foraging or migratory experience were used for standardization, they were suitable for volumetric analysis of experience-related changes in neuropil volumes. As 40-day-old animals were used, age-related developmental changes over the lifespan of a nonmigratory monarch have been allowed to occur for the standard.

When we compared the standardized sun compass neuropils with those from eight nonmigratory, summer monarchs, we observed no changes in absolute neuropil volumes, either in total volume or for individual neuropils (Fig. 2A,G). Individually analyzed neuropils included all CX components and the three largest subunits of the AOTu. We did not include the LT and the strap of the AOTu,

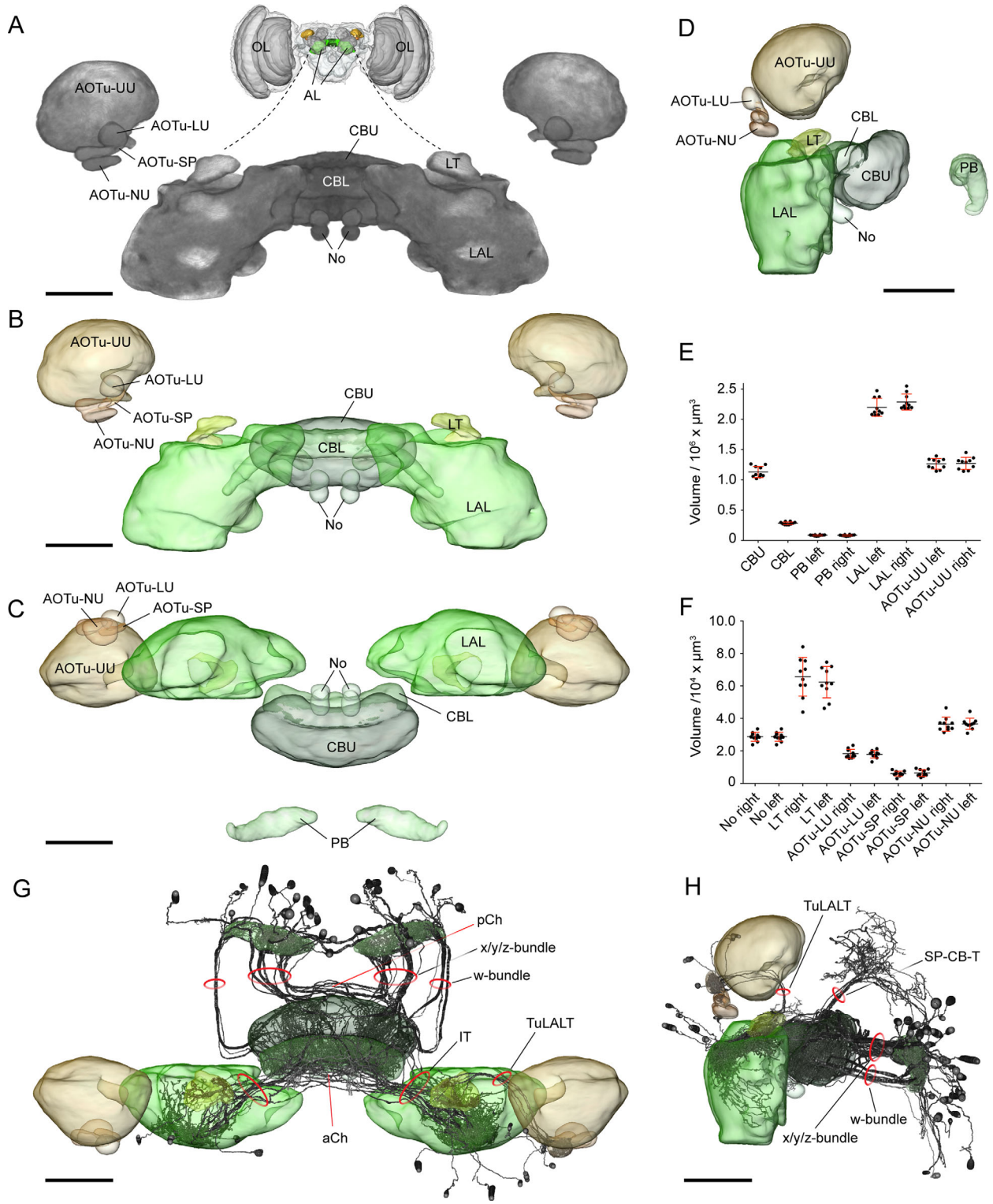

Figure 1. Standardized compass neuropils of the monarch butterfly. **A**: Frontal view of volume rendering of image stack resulting from the application of the iterative shape averaging protocol to monarch compass neuropils. The inset on top shows a frontal overview of a reconstructed monarch brain. Compass neuropils are highlighted in color. **B–D**: Surface reconstruction based on standardized label fields of compass neuropils. B, frontal view; C, ventral view; D, lateral view. **E,F**: Volumes of neuropils included for standardization. Raw values of all individual neuropils are shown (black circles), as well as the resulting mean (black line) and standard deviation (error bars). E, large neuropils; F, small neuropils. **G,H**: Illustration of the main application for the standardized compass neuropils. Columnar and tangential neurons of the central complex were registered into the common frame of reference provided by the standard, revealing major tracts and fiber bundles between different compartments of the compass neuropils. G, frontal view; tangential neurons of the upper division of the central body were omitted for clarity. H, lateral view. aCh, anterior chiasma; pCh, posterior chiasma; IT, isthmus tract; TuLALT, tubercle-LAL tract; SP-CB-T, superior protocerebrum central body tract; AL, antennal lobe; OL, optic lobe. Scale bar = 100 µm in A–D,G,H.

TABLE 2.

Mean Volumes of Compass Neuropils Used for Standardization

Neuropil	Mean absolute volume (μm^3)	SD (μm^3)	Mean relative volume (%)	Relative SD (%)
CBU	1,132,610.6	92,406.6	12.714	8.2
CBL	285,560.5	22,430.3	3.205	7.9
PB right	85,944.8	10,727.8	0.964	12.5
PB left	87,566.8	9,428.3	0.983	10.8
No right	28,720.0	2,770.9	0.323	9.6
No left	28,666.7	5,431.8	0.322	18.9
LAL right	2,275,092.8	132,427.8	25.571	5.8
LAL left	2,188,737.2	146,835.1	24.587	6.7
LT right	65,630.7	11,919.9	0.737	18.2
LT left	62,353.5	9,626.0	0.699	15.4
AOTu-UU right	1,274,912.1	99,698.8	14.315	7.8
AOTu-UU left	1,265,672.7	87,421.9	14.213	6.9
AOTu-NU right	36,425.3	4,331.3	0.409	11.9
AOTu-NU left	36,667.7	3,457.4	0.412	9.4
AOTu-LU right	18,266.3	2,743.7	0.205	15.0
AOTu-LU left	17,930.2	2,298.2	0.201	12.8
AOTu-SP right	6,020.1	1,567.0	0.068	18.2
AOTu-SP left	6,404.8	2,052.4	0.072	15.4

For abbreviations, see list.

because of their disproportionally large variability. The LAL was not included, as it does not possess a natural border outlined by a glial boundary. Because the summer butterflies were wild-caught in Massachusetts during the late summer, before the appearance of migrants, they were valid age-related controls. Thus the lack of volumetric changes in summer monarchs shows that their experience (e.g., foraging and reproductive behavior) does not affect sun compass neuropil volumes.

A different situation was found in migrants. When we compared the standard volumes with those obtained from 10 reconstructed migratory monarchs captured from Texas, we found that the migrants possessed 20–40% larger sun compass neuropils. This increase was reflected in total volume (Fig. 2G), as well as in individual neuropils (Fig. 2B), but was not reflected in the wingspan of the animals (not shown). Because not all neuropils appeared to be equally increased in size in migrants, a possible nonisometric component of the volumetric changes was analyzed. Therefore, neuropils were normalized to the total volume of compass neuropils and then subjected to the same analysis as absolute volumes. With this normalization, all CX components in migrants, except the CBU, were increased in relative size by approximately 10%, whereas the subunits of the AOTu all showed a trend toward decreased relative size by about 10%. These opposite trends were significant for the PB (increase in size) and the upper unit of the AOTu (decrease in size) (Fig. 2E). Although CX neuropils appeared to be also slightly larger in summer monarchs, no significant deviation from the standard was found (Fig. 2D).

Because the distinct changes in neuropil volumes with respect to the reference volumes in summer and migratory monarchs could be due to differences in larval/pupal development, adult age differences (migrants from Texas are likely three or more times as old as summer animals), or differences in experience, we performed additional reconstructions to differentiate these factors. First, we used five migratory monarchs netted in Massachusetts (i.e., at the beginning of their migration) in late September. Although the age of these migrants approximated that of the summer and reference animals, their reproductive status and migratory behaviors were markedly different. Next, to control for age differences, we aged five additional Massachusetts migrants housed in the laboratory in glassine envelopes for 2 months. Consequently, these aged animals were migrants of old age, but lacked the migratory experience of the Texas migrants, as they had not undergone a long-distance (>500 km) migration. Interestingly, most compass neuropils reconstructed from the young Massachusetts migrants were not different from the reference neuropils in absolute or relative volumes. Only the CBU was significantly smaller in relative volume (Fig. 2C,F,G). Surprisingly, the aged Massachusetts migrants showed an increase in absolute volumes resembling that of Texas migrants (Fig. 2C,G). However, they did not exhibit any corresponding changes in relative neuropil size (Fig. 2F). Direct comparison of the relative volume of the PB between old and young Massachusetts migrants with Texas migrants revealed a significantly larger PB only in Texas migrants. Thus, the larger PB does not correlate with migratory status or age, but does correlate with migratory experience (Fig. 2H).

To further characterize the volume differences between Texas migrants and aged Massachusetts migrants, we analyzed the allometric relationship of selected neuropil volumes with respect to the sum of the remaining compass neuropils (Fig. 2I–K). For the PB, all animals without migratory experience (i.e., standard, summer, old, and young Massachusetts migrants) followed an identical linear relationship (no difference in elevation or slope), whereas the Texas migrants followed a linear relationship that was significantly shifted to higher values, but with an identical slope (Fig. 2I). This confirmed that Texas migrants, despite having increased absolute neuropil volumes similar to those of the age-matched Massachusetts migrants, had undergone a consistent increase in PB size that was not a result of their prolonged lifespan but was correlated with migratory experience. Highlighting the specificity of this observation, regression analysis of the upper unit of the AOTu showed a shift of the regression line to lower values in the Texas migrants (Fig. 2K), whereas the CBU did not show any obvious difference between Texas migrants and the other groups

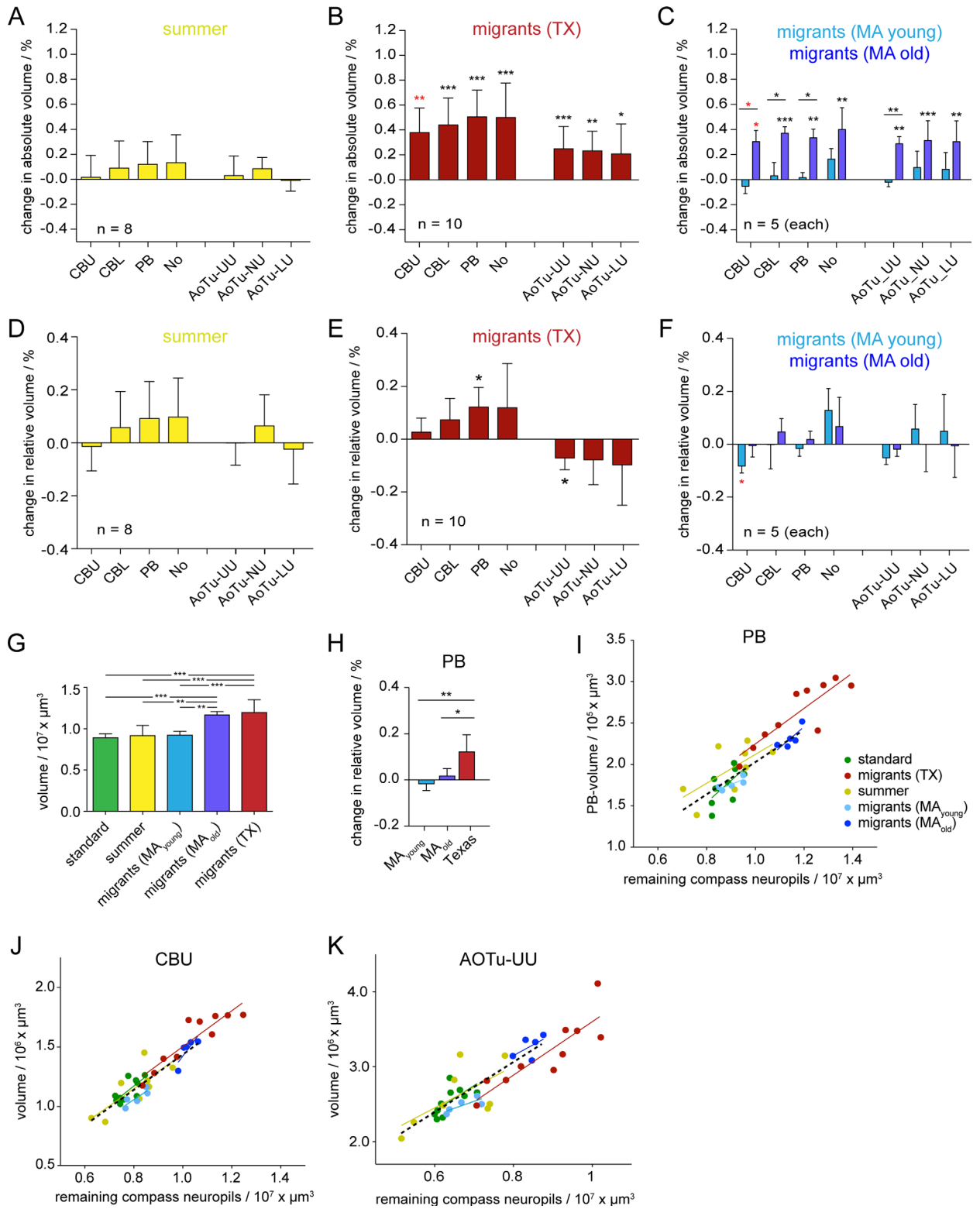

Figure 2. Volumetric comparison between standardized compass neuropils with corresponding neuropils in summer and migratory monarchs. **A–C**: Deviations of absolute volumes from standardized reference volumes. **D–F**: Deviations of relative volumes (normalized to total compass neuropils) from the corresponding relative reference volumes. **G**: Total volumes compared across all groups of butterflies. **H**: Comparison of deviations of relative PB volumes from the standardized PB volume in the different groups of migratory monarchs. **I–K**: Allometric relation of volumes of the PB (I), the CBU (J), and the upper unit of the AOTu (K) to the sum of all remaining neuropils. Solid lines are regression lines for the individual groups of monarchs (Texas migrants and standard animals: slopes significantly different from zero, $P < 0.05$; remaining groups: $P \leq 0.10$). Dashed lines are regressions of all groups of butterflies without migratory experience combined (significant in all cases, $P > 0.01$). Within a given neuropil, the slopes of regression lines are not significantly different between any groups. Regression line of Texas migrants is significantly shifted toward larger values with respect to all remaining animals for the PB ($P < 0.01$). Bars show mean ± standard deviation. Significant values are marked by asterisks (*, $P < 0.05$; **, $P < 0.01$; ***, $P < 0.001$); red asterisks indicate that nonparametric statistics were used; TX, Texas; MA, Massachusetts.

(Fig. 2J). These analyses substantiate the suggestion that experience-dependent processes orchestrate changes in volumes of brain regions linked to migratory behavior.

Major pathways of information flow linking sun compass neuropils

To address likely functional links between sun compass neuropils, we visualized many registered neurons simultaneously (Fig. 1G,H). Consequently, several prominent fiber bundles and tracts emerged that revealed the major pathways of information flow between the compartments of the compass neuropils. The largest such fiber bundles are the isthmus tracts (ITs) connecting the central body with the LALs on either side of the midline. They contain the main neurites of CBL tangential neurons, axons of CX columnar neurons with LAL projections, and major neurites of some CBU tangential neurons. Medially, the isthmus tracts merge with the anterior chiasma (aCh), a prominent fiber plexus anterior to the CBL. On the posterior side, the CBU is connected to the PB via two fiber bundles in each hemisphere. The lateral one projects to columns one and two of the PB and contains columnar neurons of the w-bundle. The medial fiber bundle contains all remaining columnar cells and thus combines the classic x-, y-, and z-bundles (Williams, 1975). Two fascicles were visible in each of the medial bundles, indicating that one of the individual x-, y-, and z-bundles might be preserved within the medial bundle. Anteriorly, the medial bundle merges with the posterior chiasma (pCh), a dense plexus of midline-crossing fibers that embed the CBU on its posterior side. Another tract provides a connection between the PB hemispheres on either side of the midline (PB commissure).

Two additional fiber tracts were also prominent in the sun compass neuropils: first, the tubercle LAL tracts (TuLALTs), which connect the different subunits of the AOTu with the ipsilateral LT; and second, the superior protocerebrum central body tracts (SP-CB-Ts), which contain axons of CBU tangential neurons originating in the superior and inferior protocerebrum and approach the CBU from the dorsolateral, posterior side in either hemisphere.

Input pathways to the central complex

To understand the integrative functions of the monarch CX in the context of sun compass navigation, the potential sources of information reaching the different CX components were analyzed. The major class of neuron proposed as CX input cells is composed of tangential cells, which connect a diverse set of brain regions to distinct compartments of the CX in many species (Schildberger, 1983; Homberg, 1985, 1994; Hanesch et al., 1989; Müller et al., 1997; Li et al., 2009; Young and Armstrong, 2010). Particularly well studied is the input pathway involved in polarized light processing. In all species studied to date (locust, honey bee, bumble bee, monarch butterfly), tangential cells from the CBL appear to receive input from AOTu projection neurons (Träger et al., 2008; Heinze and Reppert, 2011; Mota et al., 2011; Pfeiffer and Kinoshita, 2012). Both types of neuron overlap in the LT, where they form highly specialized synaptic complexes, described in detail in the locust (Träger et al., 2008). This pathway is thus of special interest for unraveling the neuronal mechanism of sun compass navigation in the monarch and was the one studied in most detail.

Parallel pathways from the anterior optic tubercle.

Recently, the detailed layout of the monarch AOTu has been described, revealing four distinct components: the upper unit, the lower unit, the nodular unit, and the strap (Heinze and Reppert, 2012). Compass-related stimuli have been shown to be processed in one or several of the small subunits of the monarch AOTu (Heinze and Reppert, 2011), consistent with data from the locust, showing that polarization-sensitive neurons are restricted to the lower unit (Pfeiffer et al., 2005; Homberg et al., 2011). Thus, only neurons innervating the three small units of the monarch AOTu were investigated in the current work.

We found three types of AOTu-associated cells, termed TuLAL1a, TuLAL1b, and TuTu neurons (according to Pfeiffer et al., 2005; Heinze and Reppert, 2011). TuLAL neurons project from the AOTu to the LT, whereas TuTu neurons connect the ipsilateral AOTu to its contralateral counterpart (Fig. 3). The somata of TuLAL neurons are located near the anterior surface of the brain, dorsal to the antennal lobe and lateral to the mushroom body lobes. Their primary neurites project posteriorly and join the main neurite of the cell close to the AOTu. The main neurite innervates one of the small subunits of the AOTu, whereas on its other end it joins the tubercle-LAL tract and enters the LT from the dorsal side (Fig. 3A,B). The two types of TuLAL1 neurons differ in the innervated AOTu subunit and the LT compartment they project to (Fig. 3C–P): TuLAL1a cells (identified in 13 examples [$n = 13$]) possess arborization trees in the strap and the nodular unit, whereas TuLAL1b cells ($n = 11$) are restricted to the lower unit of the AOTu. High-resolution analysis of both subtypes revealed a variety of shapes in their proposed input arborizations. Rather than innervating an AOTu subunit completely, fibers were restricted to sharply defined regions within these subunits. TuLAL1a neurons innervated distinct regions of the strap or were restricted to the medialmost portion of the dorsal compartment of the nodular unit (Fig. 3G–J).

Similarly, TuLAL1b cells innervated either a comparably large dorsal region of the lower unit, or were restricted to small, almost rectangular regions in variable parts of the lower unit (Fig. 3C–I). In the LT, terminals of TuLAL1a cells were confined to an anterioventral segment, whereas TuLAL1b cells exclusively innervated a posteriodorsal segment (Fig. 3K,N,O). Detailed imaging of TuLAL1 axon terminals in the LT revealed large, club-like endings with cup-shaped inundations. Two to three of these specialized structures were present in each neuron. In preparations with colabeled CBL tangential (TL) neurons, the cup-shaped openings of TuLAL1 terminals engulfed the proposed dendritic endings of the TL neurons (Fig. 3L,M).

Two examples of TuTu neurons were found (Fig. 3Q–S). They connect the lower unit and medial parts of the strap of one hemisphere to their contralateral counterparts.

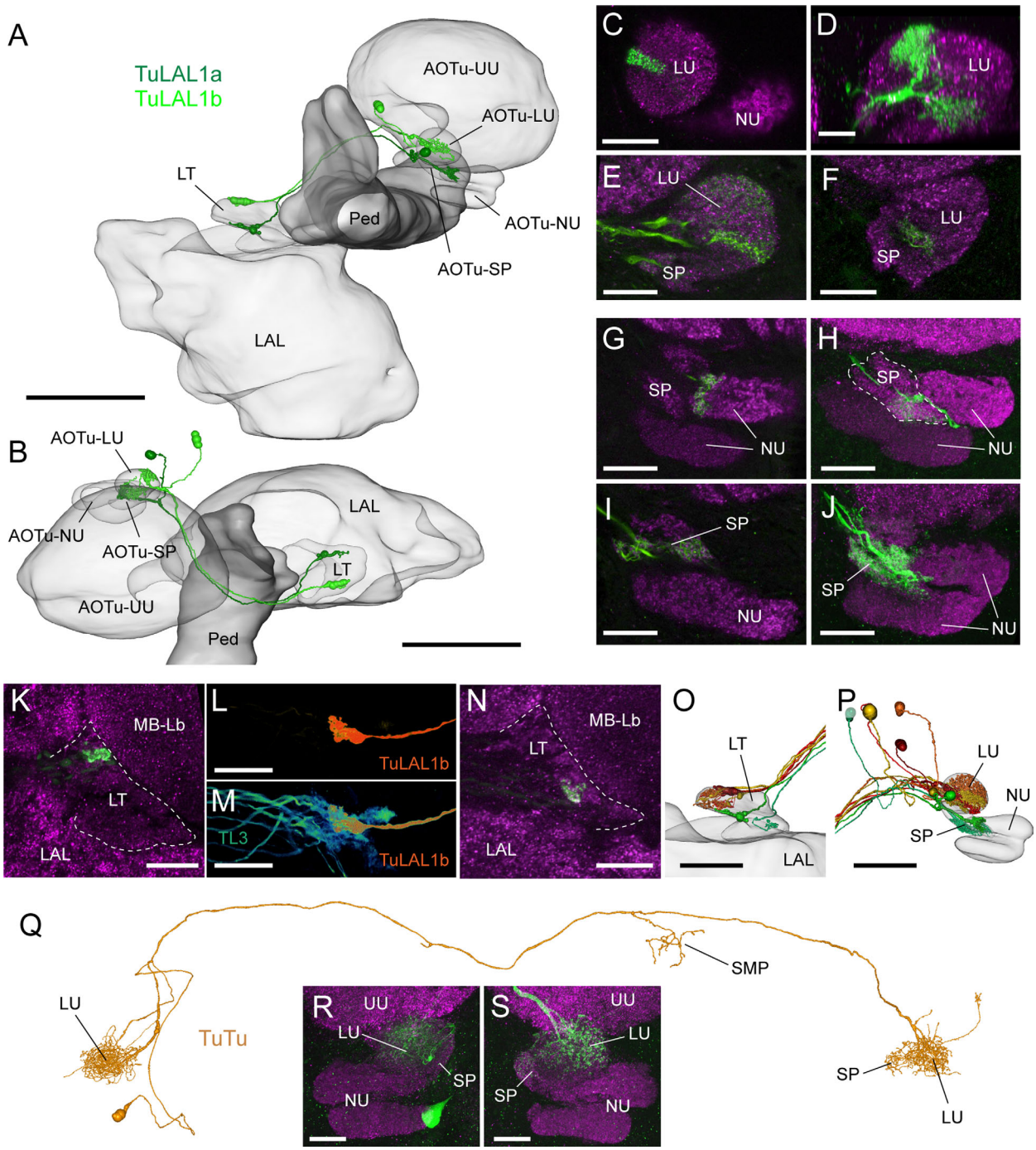

Figure 3

The soma of the fully reconstructed example was located just ventral of the AOTu, from where the primary neurite ran toward the LAL, bent dorsally, and joined the midline-crossing neurite posteriodorsally of the AOTu. Ipsilateral arborizations consisted of fine tangles of fibers, filling the innervated regions of the AOTu completely (Fig. 3R). Contralateral ramifications were clearly beaded and formed a loose mesh of fibers. Varicosities located in the lower unit were considerably larger than those in the strap (Fig. 3S). The midline-crossing neurite ran posteriorly along the dorsal brain surface and provided some additional beaded output fibers to the contralateral superior medial protocerebrum.

Tangential neurons of the CBL.

Five types of tangential neurons were found innervating the CBL, termed TL1, TL2a, TL2b, TL3, and TL4, according to the nomenclature system of the desert locust (Müller et al., 1997) (Fig. 4). All of these cell types have their proposed input arborizations within different compartments of the LAL (except for TL2a/b neurons, which share an identical input region). They have their main neurite running through the isthmus tract and projecting to single layers of the CBL, in which they define the stratified nature of this neuropil (Fig. 4L–P). Of these five types of neuron, TL2a and TL3 cells have been introduced previously through their function in the processing of skylight compass cues (Heinze and Reppert, 2011). These two cell types were also found most frequently (TL2a: $n = 23$; TL3: $n = 33$) and are hence described in the most detail. Both have their cell bodies located in the anterior protocerebrum within two clusters of somata near the anterior brain surface, close to the antennal lobes. Their primary neurites run posteriorly along the ventral face of the mushroom body lobes and reach the LT, where locally restricted parts of this neuropil are filled with presumably postsynaptic fibers (Fig. 4F–K). These very dense arborizations are characterized by a glomerular appearance with very fine fibers protruding from these glomeruli. Interestingly, endings of TL2a neurons were always restricted to the anterioventral sector of the LT, whereas TL3 projections occupied the posteriodorsal sector, effectively subdividing the LT into separate compartments and mirroring the segregation found in TuLAL1 neuron projections. The CBL projections had a beaded appearance in both types of neuron, but filled either a thin layer on the ventral side of the CBL (layer 2; TL2a) or occupied a tube-like layer in the CBL center (layer 3; TL3) (Fig. 4N,O).

The remaining three types of TL cells were found less frequently (TL1: $n = 1$; TL2b: $n = 6$; and TL4: $n = 1$). TL2b cells were similar to TL2a neurons with respect to location of somata and LT input arborizations (Fig. 4C). However, ramifications in the LT appeared less extensive and were restricted to the ventrolateral extreme of the neuropil (Fig. 4J). In the CBL, TL2b cells possessed terminals on the dorsoposterior side of the CBL (layer 4) as opposed to the ventral side in TL2a cells (Fig. 4M). TL1 and TL4 neurons were found as individual examples only, but were clearly distinct from the other types of TL neurons. They did not innervate the LT, but fibers of the TL1 cell filled the anterior loblet of the LAL (Fig. 4D), whereas the TL4 neuron only possessed very few, thin fibers stretching along the anterior surface of the dorsal LAL (Fig. 4E). Although the location of the soma of the TL4 cell was similar to that of the remaining TL neurons, the TL1 cell had its soma in the ventromedial protocerebrum, close to the oesophagus. The major neurites of TL4 projections were located close to the ventral CBL surface and gave rise to thin processes that formed a loose mesh

Figure 3. Input neurons originating from the anterior optic tubercle (AOTu). **A,B**: 3D reconstruction of representative examples of one TuLAL1a and one TuLAL1b neuron, registered into the standardized compass neuropils. The mushroom body pedunculus was included by affine registration of an individual central-brain reconstruction. A, frontal view; B, dorsal view. **C–F**: Confocal images of three preparations containing neurobiotin-injected TuLAL1b neurons (green) colabeled against synapsin (magenta). Shown are arborization domains in the lower unit of the AOTu. D contains two neurons. D is ventral view of the same preparation as C, revealing two ramification domains of this neuron. C–E, frontal views. **G–J**: As C–E, but arborizations of TuLAL1a neurons are shown. I, mass injection of three to five neurons. **K**: Terminal of a single TuLAL1b neuron in the dorsal sector of the lateral triangle (LT) (neuron: green; synapsin labeling: magenta). **L**: Volume rendering of TuLAL1b terminal in the LT, revealing the cup-shaped structure of axonal endings. **M**: Same preparation as L, but visualization includes colabeled tangential neurons (TL3) of the lower division of the central body, showing spatial proximity of postsynaptic regions of TL3 neurons and presynaptic terminals of TuLAL1b neurons. **N**: Terminal of a single TuLAL1a neuron in the ventral sector of the LT (neuron: green; synapsin labeling: magenta). **O**: Mapping of arborizations of two TuLAL1a neurons (green) and five TuLAL1b (red and yellow) in the LT, revealing spatially segregated output regions in dorsal and ventral regions of the LT. **P**: Mapping of arborizations of TuLAL1 neurons in the AOTu; same neurons as shown in O. Whereas TuLAL1a neurons are restricted to the strap region and small parts of the nodular unit, TuLAL1b neurons occupy distinct, largely non-overlapping compartments of the lower unit (colors as in O). **P**: 3D reconstruction of a neuron connecting the ipsilateral and the contralateral AOTu (TuTu neuron). Beaded side branches are also located in the superior medial protocerebrum (SMP). **Q,R**: Confocal images of ipsilateral arborizations (Q) and contralateral arborizations (R) illustrate the presence of smooth endings in the ipsilateral ramifications and varicose terminals in contralateral ramifications. Fibers are restricted to the lower unit and parts of the strap region. Scale bar = 100 μm in A,B; 50 μm in O,P; 20 μm in C,E–N,R,S; 10 μm in D.

of finely beaded terminals filling layer 1 and partly extending into layer 2 (Fig. 4E,P). TL1 processes were restricted to layer 2 of the CBL.

Tangential neurons of the CBU.

In contrast to the limited number of neurons providing input to the CBL from locally restricted regions of the

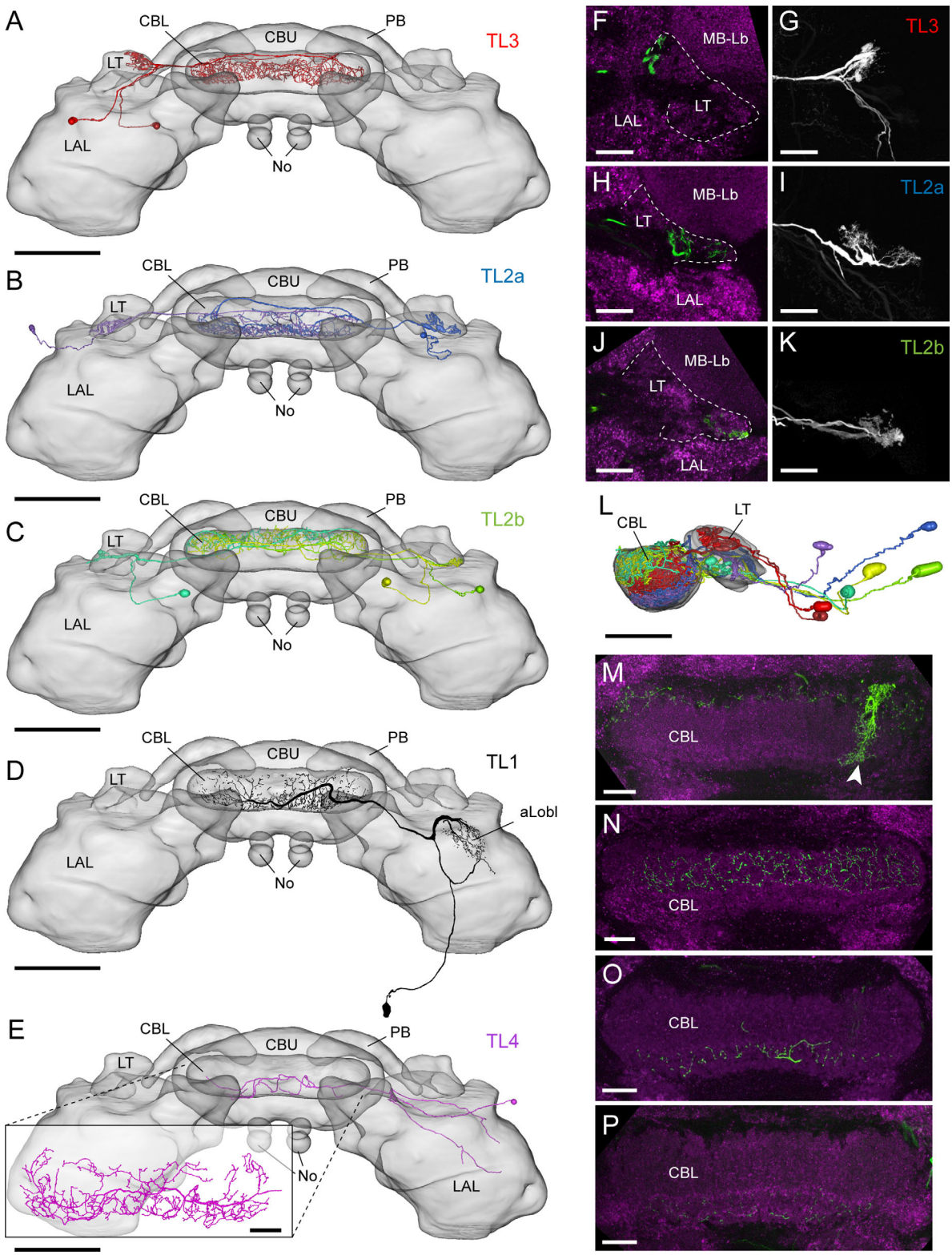

Figure 4

LAL, the proposed input neurons of the CBU represent a large, diverse set of neurons connecting this neuropil to many regions of the central brain (Fig. 5, Table 3). In the current work, we identified individual examples of 13 different CBU tangential neurons, termed TU cells. They were classified into three groups based on the location of their somata. Six neurons had somata located in the posterior dorsolateral protocerebrum (TU-pdl neurons), three neurons were found with somata in the posterior ventromedial protocerebrum (TU-pvm neurons), and three neurons possessed somata in the anterior protocerebrum, either in the anterior ventromedial protocerebrum (TU-avm cells; $n = 2$) or in the anterior inferiomedial protocerebrum (TU-aim cells; $n = 1$). These neuron groups were further classified according to the innervated CBU layer (I to IV). To allow identification of individual cell types, numbers were added to these descriptive names in order of discovery.

All TU neurons were registered into the standard to allow them to be displayed within the same frame of reference (Fig. 5). Although fibers within the compass neuropils were mapped with the same reliability as CX intrinsic neurons, the potential error for the wide-ranging branches outside the compass neuropils was greater due to the lack of nearby landmarks. To map these arborizations onto the previously described subdivisions of the unstructured protocerebrum (Heinze and Reppert, 2012), we matched the reconstruction of a representative central brain to the standard by affine registration (matching of size and orientation; Fig. 5J,K).

The largest group of TU neurons were TU-pdl cells, i.e., neurons with somata in the posterior dorsolateral protocerebrum, just anterior and slightly lateral to the mushroom body calyx (Fig. 5A,B). The primary neurites run along the anterior face of the calyx toward the midline and bend ventrally, forming an axon bundle that approaches the CBU dorsolaterally. Several major branches emerge from the primary neurite before it reaches the CBU. These branches form a mesh of smooth arborizations covering extensive areas in one or two regions of the superior and inferior protocerebrum. TU-pdl neurons innervating CBU layers I and II possess major neurites that cross the midline on the anterodorsal side of the CBU, while giving rise to multiple, regularly spaced branches that penetrate the CBU surface and form dense arborizations in one CBU layer (Fig. 5C). These arborizations are clearly beaded and span the complete innervated layer. TU-pdl neurons projecting to CBU layer IV possess major neurites that continue to run anteriomedially after reaching the posterior edge of the CBU, wrap around the CBL, and give rise to several branches that enter the CBU anteriorly. These fan-shaped branches form arborizations with beaded terminals in substrata of CBU layer IV (Fig. 5C). No TU-pdl neurons innervating CBU layer III were identified.

The second group of TU cells with posteriorly located somata are TU-pvm neurons (ventromedial somata). The three reported cells show little resemblance to one another and connect diverse regions of the brain with CBU layers III and IV (Fig. 5D–F). The first neuron (TU-pvm-(III)-1) possessed a primary neurite that ran dorsally toward the lateral end of the PB, continued anteriorly, and entered the posterior region of the superior posterior inferior protocerebrum (SPIP). Here, the neurite branched several times, giving rise to three major fibers. The first one innervated parts of the superior medial protocerebrum (SMP; dorsal shell, minor branches in ventral shell). The second fiber ran anteriorly through the inferior protocerebrum (SPIP and anterior inferior protocerebrum [AIP]), providing sparse innervation of these regions. The third fiber ran toward the lateral, posterior edge of the CBU and, while crossing the midline within the posterior chiasma, sent off regularly spaced branches that gave rise to beaded terminals throughout CBU layer III (Fig. 5F). The second neuron of this group of TU cells (TU-pvm-(IV)-1) had a primary neurite that followed the course of the w-bundle toward the anteriolateral edge of the central

Figure 4. Tangential input neurons to the lower division of the central body (CBL). **A–C**: 3D reconstructions of the three most frequently identified types of CBL tangential neurons (TL neurons), registered into the standardized compass neuropils. A, TL3; B, TL2a; C, TL2b. All images are frontal views. **D**: 2D projection view of a TL1 neuron projected onto the standardized compass neuropils. **E**: 3D reconstruction of a TL4 neuron registered into the standardized compass neuropils; inset: reconstruction (unregistered) based on a high-resolution confocal scan (40× objective). **F,H,J**: Confocal images of neurobiotin-injected TL neurons (green) colabeled against synapsin (magenta), illustrating the localization of input arborizations within dorsal compartments of the lateral triangle for TL3 neurons (J) and ventral compartments for TL2a (H) and TL2b neurons (H). **G,I,K**: Maximal intensity projections of arborizations in the lateral triangle of the neurons shown in F,H,J, respectively. F/G and J/K show arborizations of two neurons of the same type. **L**: Mapping of TL neuron arborizations to distinct layers of the CBL and separate regions of the lateral triangle; same neuron and colors as in A–C (TL3, TL2a, TL2b); lateral view (anterior is to the right). **M–P**: Confocal images of neurobiotin-injected TL neurons (green) colabeled against synapsin (magenta), illustrating the distinct layers innervated by the different types of TL neurons. Layer 4 is innervated by TL2b cells (M), layer 3 by TL3 cells (N), layer 2 by TL2 cells (O), and layer 1 by TL4 cells (P). An unrelated columnar neuron was coinjected in M (arrowhead). Scale bar = 100 μm (A-E); 50 μm (L); 20 μm (inset in E, F-K, M-P).

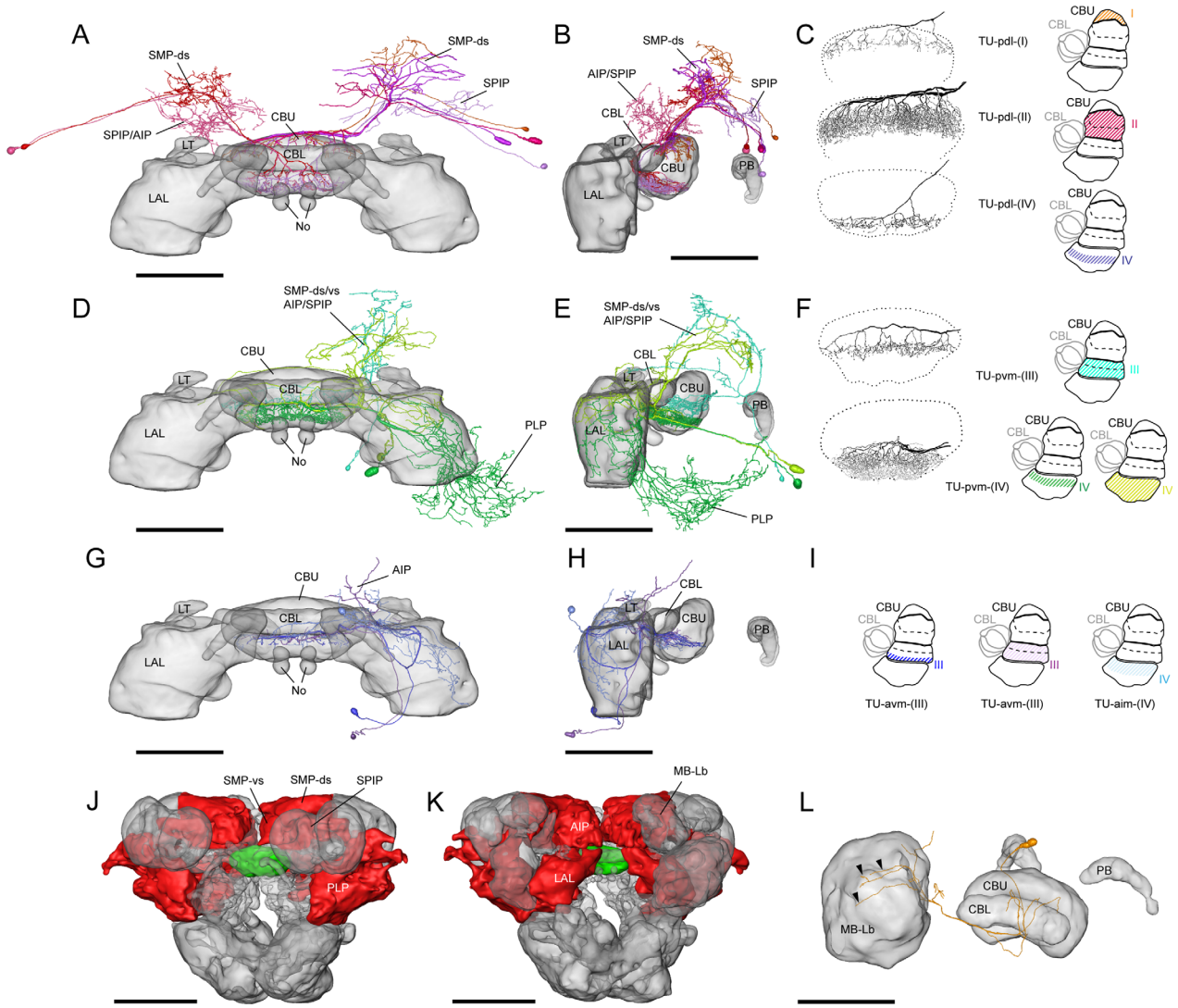

Figure 5. Tangential input neurons to the upper division of the central body (CBU). **A**,**B**: 3D reconstructions of TU neurons with somata located in the posterior dorsolateral protocerebrum (TU-pdl cells) registered into the standardized compass neuropils. (A, frontal view; B, lateral view). **C**: Innervated layers of the CBU for TU-pdl cells. Left: frontal camera lucida reconstructions; right: schematic representation of the CBU with innervated layers highlighted. **D**–**F**: As A–C, but for TU neurons with somata in the posterior, ventromedial protocerebrum (TU-pvm cells). Two different TU-pvm-(IV) cells were superimposed in one preparation and are jointly shown in F (lower reconstruction). **G**–**I**: As A–C, but for TU neurons with their somata located in the anterior protocerebrum (ventromedial: TU-avm cells; inferiomedial: TU-aim cell). No camera lucida reconstructions could be obtained due to superimposed arborizations or weak labeling in the CBU. Therefore, extent of fibers in two of the three cells is only approximate (faded hatchings). **J**,**K**: 3D reconstruction of the central brain. Regions containing input arborizations of TU neurons are highlighted in red; CBU is shown in green. (J, oblique posterior view; K, oblique anterior view). **L**: TU neuron connecting the mushroom body lobes to the CBU (not registered into the standard). Arrowheads highlight fibers innervating the mushroom body lobes. AIP, anterior inferior protocerebrum; PLP, posterior lateral protocerebrum; SMP-vs, ventral shell of superior medial protocerebrum; SMP-ds, dorsal shell of SMP; SPIP, superior posterior inferior protocerebrum. Scale bar = 150 µm in A,B,D,E,G,H,L); 300 µm in J,K.

body, at which point it split into two major neurites. The first one entered the CBU from anterior and fan-shaped fibers emerged posteriorly to innervate a substratum of CBU layer IV with beaded fibers. The second neurite ran diagonally along the posterior face of the LAL, where several fibers branched off to innervate lateral parts of the dorsal LAL. The main neurite bent posteriorly and gave rise to a major arborization tree spanning medial regions of the posterior lateral protocerebrum (PLP) all the way to the posterior brain boundary (Fig. 5D,E). The third neuron of this group (TU-pvm-(IV)-2) possessed a primary neurite that also followed the w-bundle toward the central body, at which point one major neurite branched off and innervated CBU layer IV from anterior, similar to TU-pvm-(IV)-1.

TABLE 3.

Proposed Input and Output Regions of Central-Body Tangential Neurons

Cell type	Output region	Input region
TL1	CBL-layer 2	aLobl of LAL
TL2a	CBL-layer 2	LT (ventral sector)
TL2b	CBL-layer 4	LT (ventral sector)
TL3	CBL-layer 3	LT (dorsal sector)
TL4	CBL-layer 1	dLAL
TU-pdl-(I)	CBU-layer I	SMP-ds
TU-pdl-(II)-1	CBU-layer II	SMP-ds
TU-pdl-(II)-2	CBU-layer II	SMP-ds
TU-pdl-(IV)-1	CBU-layer IV (substratum)	SPIP
TU-pdl-(IV)-2	CBU-layer IV (substratum)	SMP-ds
TU-pdl-(IV)-3	CBU-layer IV (substratum)	SPIP, AIP
TU-pvm-(III)	CBU-layer III	SMP-ds, SMP-vs, SPIP, AIP
TU-pvm-(IV)-1	CBU-layer IV (substratum)	dLAL, PLP
TU-pvm-(IV)-2	CBU-layer IV	dLAL, AIP, SPIP, SMP-ds, SMP-vs
TU-aim-(IV)	CBU-layer IV (substratum)	dLAL, AIP
TU-avm-(III)-1	CBU-layer III (border to IV)	dLAL
TU-avm-(III)-2	CBU-layer III	dLAL, AIP
TU-MB	CBU-layer ?	Mushroom body lobes, inferior PC

Abbreviations: aim, anterior inferiomedial protocerebrum; avm, anterior ventromedial protocerebrum; AIP, anterior inferior protocerebrum; pdl, posterior dorsolateral protocerebrum; PLP, posterior lateral protocerebrum; pvm, posterior ventromedial protocerebrum; SMP-vs, ventral shell of superior medial protocerebrum; SMP-ds, dorsal shell of superior medial protocerebrum; SPIP, superior posterior inferior protocerebrum; TL, CBL tangential neuron; TU, CBU tangential neuron. For other abbreviations, see list.

Additionally, several thin fibers emerged from the main neurite and ran anteriorly around the CBL, bent laterally, and innervated the AIP on both sides of the midline. Arborizations within the CBU were finer compared with the other neurons of this group and covered layer IV completely (Fig. 5F). After the main branching point, the second major neurite bifurcated again. Whereas the first fiber innervated dorsal regions of the dorsal LAL, the second fiber ran dorsoposteriorly and provided extensive projections to the AIP, the SPIP, and both shells of the SMP (Fig. 5D,E).

The last group of TU neurons contains three cells with anteriorly located somata. The first neuron (TU-aim-(IV)-1) possessed a soma located in the inferior medial protocerebrum (Fig. 5G,H). The primary neurite entered the dorsal LAL and joined the cell's major neurite, which gave rise to numerous smooth fibers innervating the complete dorsal LAL. Some branches left the LAL dorsally and projected to adjacent regions of the AIP. The main neurite entered the isthmus tract and continued toward the midline, running just ventral to the CBL. Several fibers left the main neurite posteriorly to innervate CBU layer IV. The extent of these arborizations and their appearance could not be unambiguously determined because of superimposed fibers of other TU cells. The two remaining TU cells (TU-avm-(III)-1/2) had their somata located ventromedially near the oesophagus. The primary neurites entered the LAL ventrally and traversed the neuropil at the boundary of the dorsal and ventral LAL, until they joined the isthmus tract. In the LAL, the first cell possessed one major branch that gave rise to fibers in the anteriodorsal region of the dorsal LAL, whereas the second cell possessed arborizations in the dorsalmost regions of the dorsal LAL, as well as in adjacent areas of the AIP. Both main neurites crossed the midline just ventral to the CBL and gave rise to fan-like fibers that entered the CBU from the anterior. Arborizations of cell one were restricted to a thin layer at the boundary of CBU layer III and IV, whereas cell two innervated layer III more broadly.

Finally, a neuron was found that connected the mushroom body lobes with the CBU (Fig. 5L). The soma of this neuron was posterior, near the midline, adjacent to the PB. Arborizations were found in the CBU, in the inferior protocerebrum adjacent to the mushroom body lobes, and in the mushroom body lobes themselves. Due to incomplete staining, the CBU arborizations could not be fully traced and the remaining arborizations are likely incomplete. Nevertheless, this neuron indicates the existence of a direct connection between the mushroom body and the monarch CX.

Other tangential neurons.

Only one example of a wide-field tangential neuron innervating regions of the CX other than the central body was encountered (TB-avm-1; Fig. 6A,B). This neuron connected the LAL and the PLP to the PB. Its soma was located in the anterior, ventromedial protocerebrum, adjacent to the oesophagus. The primary neurite projected posteriorly and bifurcated just before reaching the posterior brain surface. One major neurite ran laterally and, before extending further anteriorly, gave rise to arborizations in the PLP. It entered the LAL from the posterior side and arborized at the boundary of the dorsal and ventral LAL. The second major neurite continued dorsally from the branching point of the primary neurite until it reached the PB. It bifurcated and innervated both halves of the PB with a dense mesh of fibers.

Columnar neurons and intrinsic elements of the central complex

As opposed to the previously described wide-field tangential neurons, whose projections span the whole width of one of the CX components, all the following cell types possess arborization trees restricted to CX columns, either in the PB, the CBU, or the CBL. These cells provide

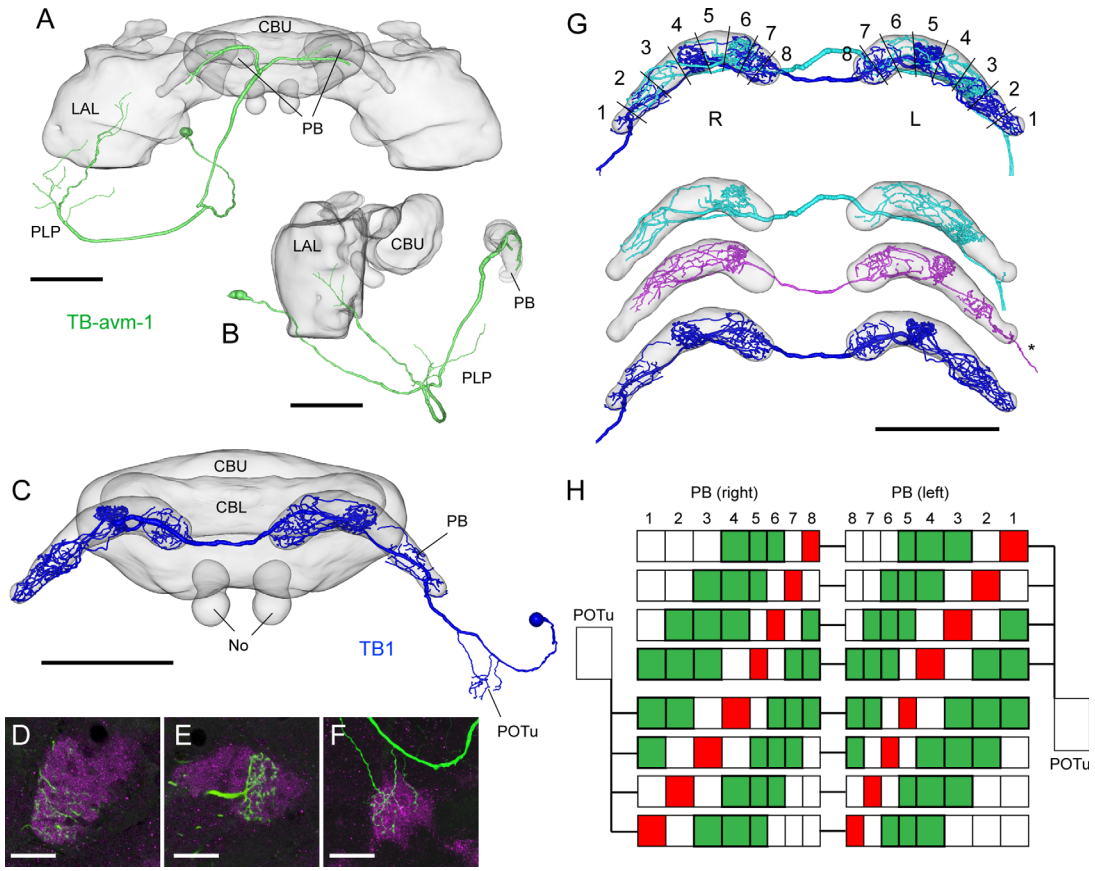

Figure 6. Tangential neurons of the protocerebral bridge. **A,B**: Tangential neuron of the PB with input fibers in the LAL and the posterior lateral protocerebrum (PLP) (A, posterior view; B, lateral view). Only major arborizations are shown due to superposition of fibers from other neurons. **C**: 3D reconstruction of a TB1 neuron registered into the standardized central complex (posterior view). **D–F**: Confocal images of arborization domains in the protocerebral bridge (PB; D,E), and the posterior optic tubercle (POTu; F). Varicose fibers are found in one column of the PB in either hemisphere (E), whereas smooth fibers are found in other columns (D). Small varicosities are also present in the POTu (F). Anti-synapsin labeling (magenta) is superimposed with the neurobiotin-injected neuron (green). **G**: Distribution of fibers in columns along the PB. Top: two TB1 neurons are superimposed, illustrating the location of varicosities (R4/L5; R6/L3). Bottom: three examples of TB1 neurons. The asterisk marks a neuron that does not fully match the connectivity scheme shown in H. **H**: Heterolateral connectivity scheme adapted for the monarch from locust data (Heinze and Homberg, 2007). Each row indicates an individual neuron, whereas rectangles indicate PB columns (numbering as in G). Green squares show columns filled with proposed input fibers, and red squares show proposed output regions. Scale bar = 100 μm in A,E,G; 20 μm in B–D.

the substrate for information flow between the different CX components and exhibit complex interhemispheric connectivity patterns. In total, we were able to identify one type of multicolumnar neuron of the PB, three types of pontine neuron of the CBU, six types of columnar neurons of the CBU, and three types of columnar neurons of the CBL. The somata of all cell types are located close to the PB near the posterior brain surface.

Multicolumnar neurons of the PB.

In the monarch PB a cell type with a remarkably complex projection pattern was recently identified (Heinze and Reppert, 2011). Here, we found additional examples of this type of neuron and were able to describe its morphology in detail (Fig. 6). Generally, these cells innervate distinct sets of PB columns with either varicose or smooth arborizations and additionally project to the posterior optic tubercle (Fig. 6C), a small neuropil at the posterior brain boundary (Heinze and Reppert, 2012) (Fig. 6D–F). In accordance with the locust and owing to the tangentially oriented main neurite, it was termed TB1 neuron (Heinze and Homberg, 2007). One PB column on either side of the midline is filled with thick, varicose terminals, approximately eight columns apart from each other (Fig. 6G). Because medial PB columns in the monarch were narrower than lateral columns and the neurons we found innervated mostly medial columns, the distance between the varicosities spanned only between 34% and 39% of the total PB width. The columns on either side of the varicosities largely lacked ramifications, whereas most of the

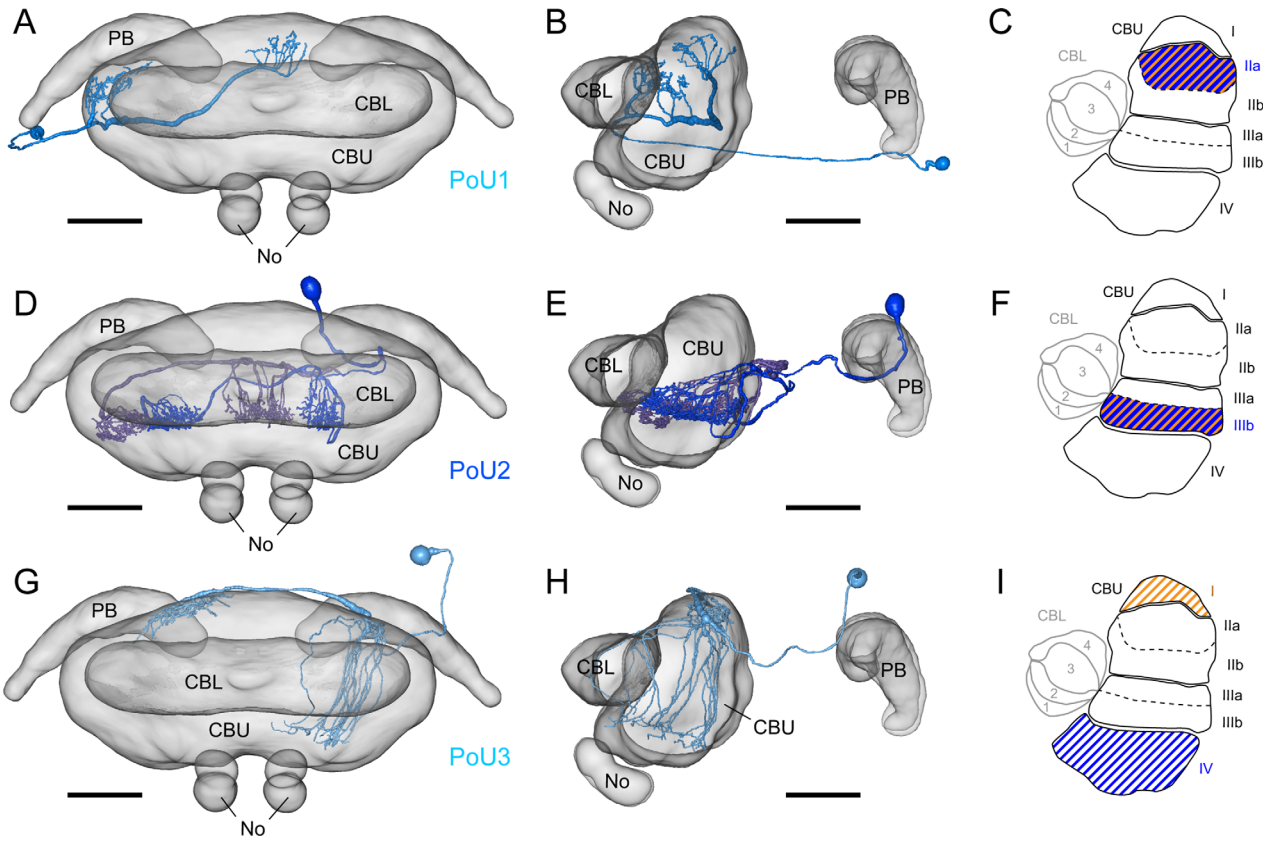

Figure 7. Pontine neurons of the CBU. **A,B**: 3D reconstruction of a PoU1 neuron innervating layer II of the CBU, registered into the standardized central complex (A, frontal view; B, lateral view). **C**: Schematic illustration of innervated layers (lateral view). Proposed input and output regions are illustrated by blue and orange hatching, respectively. **D–F**: As A–C, but for two PoU2 neurons. **G–I**: As A–C, but for a PoU3 neuron. For abbreviations, see list. Scale bar = 50 μm in A,B,D,E,G,H.

remaining columns were filled with a loose mesh of smooth terminals. Finally, the fibers observed in the posterior optic tubercle possessed small varicosities, but were not highly developed in number and density (Fig. 6F). From the observed neurons, together with homologous neurons reported from the locust (Heinze and Homberg, 2007), we extrapolated a heterolateral connectivity scheme for monarch TB1 neurons (Fig. 6H). Although registration into the standard showed that this scheme was generally observed by the identified neurons, the variable width of the PB columns and the variability in overall PB shape appeared to introduce inaccuracies in the relative location of the varicose columns between individual neurons. Hence, the heterolateral connectivity scheme should be considered an idealized version.

Pontine neurons.

Aside from tangential and columnar neurons, the insect CX contains a third major class of neurons, the pontine cells. Three types of pontine cells were identified in the monarch CX, termed PoU1, PoU2, and PoU3, all of which were restricted to the CBU (Fig. 7). While only an individual PoU3 neuron was found, PoU1 and PoU2 cells were found twice. Originating from the somata, the primary neurites of all pontine cells bypass the PB, bifurcate before entering the CBU, and connect two columnar arborization domains in either CBU hemisphere. Ipsilateral arborizations were generally of smooth appearance, whereas contralateral arborizations showed varicosities. All projections of the PoU1 cells were restricted to layer IIa (Fig. 7A–C). In the reconstructed example, the ipsilateral arborization was located in the lateralmost column and the contralateral arborization in the column adjacent to the midline (Fig. 7A). The midline-crossing neurite ran along the posterior face of the CBU, a path also followed by PoU2 neurons. PoU2 neurons innervated layer IIIb with both arborization trees, each of which covered approximately one-fourth of one CBU hemisphere (Fig. 7D–F). The two stained PoU2 neurons innervated different pairs of columns on either side of the midline, indicating an isomorphic set of neurons covering all CBU columns. Extrapolating from the width of the arborization trees, a set of eight PoU2 neurons could cover the complete CBU (Fig. 7D).

The last example of pontine cell, the PoU3 neuron, had a more complex appearance, as the proposed input and output arborizations were not located in the same CBU layer (Fig. 7G–I). The ipsilateral arborization tree consisted of straight fibers that originated at the dorsal CBU surface and orthogonally penetrated all layers. They terminated in fine fibers that spread laterally in dorsal regions of layer IV, filling this area with a dense mesh of very fine terminals. The contralateral arborization tree was heavily beaded and located in layer I, directly underneath the CBU surface. In contrast to the other types of pontine cells, the midline-crossing neurite was located on the dorsal side of the CBU.

Columnar neurons of the CBL.

Three types of columnar neurons innervating the CBL were found in the monarch (Fig. 8). They were termed CL1a, CL1b, and CL2 cells (Müller et al., 1997; Heinze and Homberg, 2008). CL1 neurons ($n = 10$) connect single columns of the PB and the CBL with the anterior loblet, a region recently defined as a distinct compartment of the monarch LAL (Heinze and Reppert, 2012). Coming from the soma, the primary neurite of CL1 cells projects to one PB column, continues to the posterior CBU surface, and transects the CBU toward the CBL, giving rise to dense fibers filling one CBL column (Fig. 8D–G). It continues anteriorly around the CBL and joins the contralateral isthmus tract toward the anterior loblet, where a loose mesh of beaded fibers evenly fills this structure (Fig. 8L–O). Midline crossing occurs either in the posterior chiasma (cells projecting to contralateral CBL columns) or in the anterior chiasma (neurons innervating ipsilateral CBL columns). Although four of the 10 CL1 cells found could not be reconstructed in their entirety, because either the connection to the LAL or, in one case, the connection to the PB was not traceable, we could infer a heterolateral connectivity scheme consisting of a set of 16 neurons (Fig. 8C). In this bilaterally symmetrical system, each PB hemisphere is projected onto the width of the CBL, so that the medialmost PB column of one brain hemisphere (e.g., R1) and the lateralmost PB column of the other brain hemisphere (L8; and corresponding pairs of remaining PB columns: R2/L7, R3/L6, etc.) are connected to overlapping CBL columns.

Based on the appearance of the arborization trees in the PB and the CBL, we distinguished two CL1 subtypes, termed CL1a and CL1b. One example of each subtype was examined in more detail in rehydrated thick sections, confirming the distinct nature of these neurons. In the CBL, the CL1a cell was largely restricted to a narrow domain spanning no more than one column. It extended laterally into neighboring columns only in ventral and dorsal parts of the CBL. In these regions, particularly in layer 4, fiber terminals were much denser (Fig. 8D,E). In contrast, the CL1b neuron possessed much wider CBL arborizations, suggesting considerable overlap between neighboring columns. The cross-section of the CBL was uniformly filled with clearly beaded terminals, with the exception of layer 4, which appeared to be free of fibers (Fig. 8F,G). In the PB, the CL1a neuron possessed an arborization tree characterized by thick varicosities and sparse innervation, whereas the CL1b cell possessed a much denser mesh of terminals without clear varicosities (Fig. 8H–K). Surprisingly, the diameter of the major fiber connecting the CBL with the PB was considerably smaller compared with the fiber serving the LAL in both examples. No differences between the subtypes were observed in the innervation pattern to the anterior loblet of the LAL. Here, although they spanned the whole structure, both subtypes almost completely avoided the dense foci of anti-synapsin labeling described as microglomeruli (Heinze and Reppert, 2012; Fig. 8M,O).

Four examples of CL2 neurons were found, two of which could not be traced to the PB (Fig. 8P–R). These cells connect columns of the PB and the CBL to layer 1 of the contralateral nodulus. After giving rise to a columnar arborization in an ipsilateral PB column, the main neurite continues toward the posterior chiasma, transects the CBU towards the CBL, and bifurcates into two fibers. The first one gives rise to a columnar arborization concentrated in ventral CBL layers (Fig. 8R), whereas the second one projects to the contralateral nodulus, where it densely innervates the cap-like layer 1. Midline crossing occurs either in the posterior chiasma (neurons projecting to a contralateral CBL column) or in the neurite projecting to the nodulus (neurons innervating ipsilateral CBL columns). The CL2 cells identified suggest the existence of an isomorphic set of neurons, but because only two examples of completely reconstructed neurons were available, we did not attempt to infer their heterolateral arborization scheme.

Columnar neurons of the CBU.

Six types of columnar neuron were found innervating the CBU (Figs. 9, 10). Of these, three types connected columnar regions of the PB and the CBU to the dorsal LAL and were termed CPU1a, CPU1b, and CPU2 neurons (Heinze and Homberg, 2008; Heinze and Reppert, 2011). These neurons are characterized by large-fiber diameters and possess a clear polarity, with fine arborizations located in the PB and CBU, and large varicosities in the LAL (Fig. 9). In CPU1a neurons ($n = 8$) the primary neurite gives rise to an arborization tree covering one ipsilateral PB column (Fig. 9A,O). The main neurite then enters one of the fiber bundles connecting the PB with the CBU and runs toward the posterior CBU surface. Here it sends fine fibers into a columnar arborization domain of the CBU,

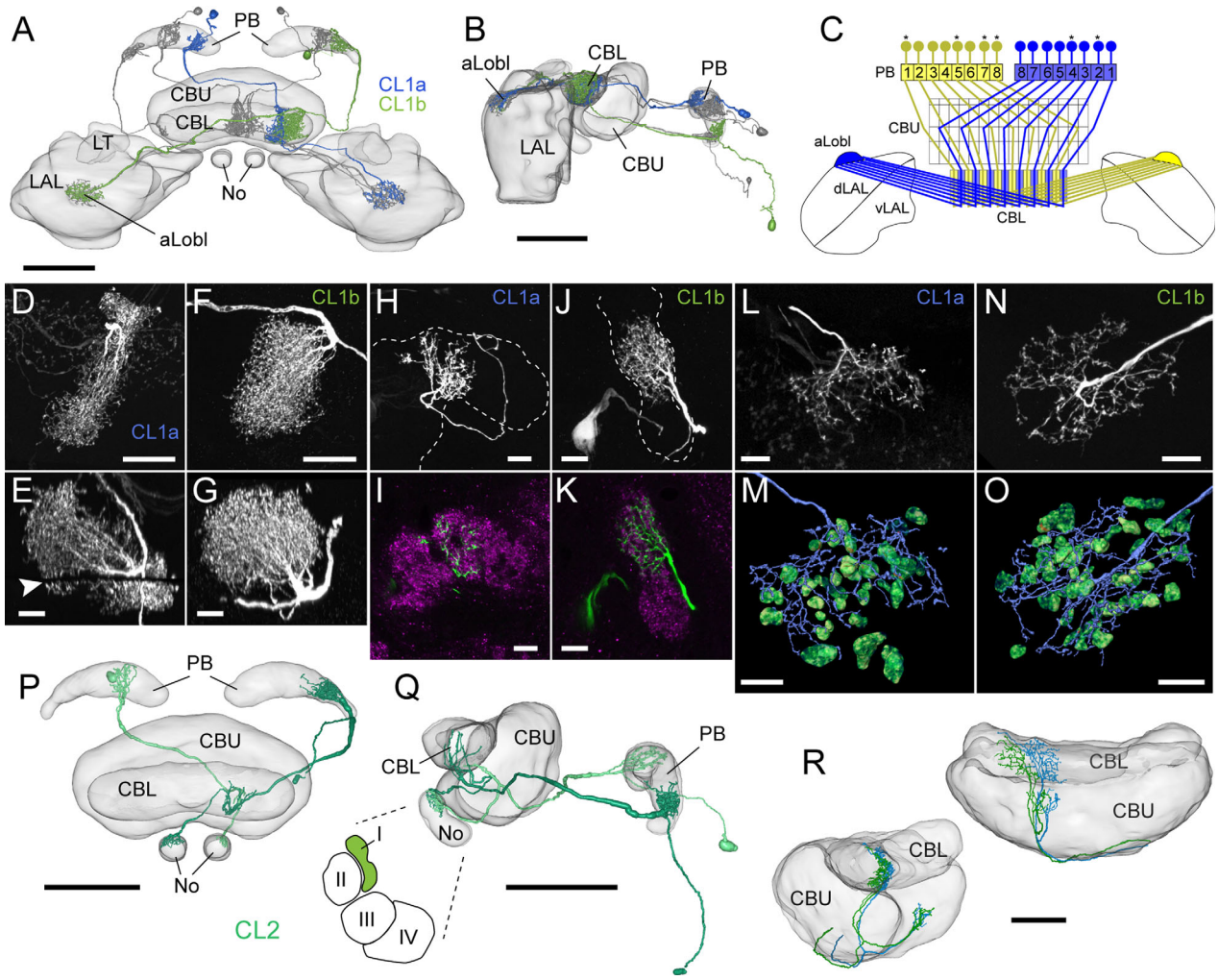

Figure 8. Columnar neurons of the CBL. **A,B**: 3D reconstruction of five CL1 neurons, registered into the standardized compass neuropils. One CL1a neuron is highlighted in blue, and one CL1b neuron is shown in green (A, frontodorsal view; B, lateral view). **C**: Schematic representation of the proposed heterolateral connectivity scheme of CL1 neurons. Identified neurons are marked by an asterisk. **D,E**: Confocal images of CBL arborizations of a neurobiotin-injected CL1a neuron. The images are composites of two maximal intensity projections of adjacent brain sections (D, frontal view; E, lateral view). The arrowhead indicates lost tissue at the boundary of the two frontal sections. **F,G**: Confocal images of CBL arborizations of a CL1b neuron (F, frontal view; G, lateral view). Note the varicose nature of fibers. **H**: Confocal image of PB arborization of a CL1a neuron. PB outline is shown as dashed line. **I**: Detailed view of H revealing the varicose nature of fiber terminals (synapsin-ir, magenta; injected neuron, green). **J,K**: As H/I, but for CL1b neuron. **L**: Confocal image of a CL1a neuron arborization tree in the anterior loblet of the LAL (aLobl). **M**: Surface reconstruction of the arborization tree shown in H, together with reconstruction of microglomeruli of the anterior loblet. Local synapsin immunoreactivity of the image stack has been projected onto the reconstructed microglomeruli. Neural branches colocalizing with microglomeruli are displayed in red, and remaining branches are shown in blue. Note that the neurites almost entirely avoid the microglomeruli. **N,O**: As L/M, but for CL1b neuron. **P,Q**: 3D reconstruction of two CL2 neurons registered into the standardized central complex (P, frontal view; Q, lateral view). CBL arborizations were superimposed by other neurons so that the reconstruction is restricted to major branches. **Inset in Q**: Schematic illustration of innervated nodulus layer. **R**: 3D reconstruction of two CL2 neuron fragments, revealing the innervated layer and the extent of arborizations in the CBL (left, oblique view; right, ventral view). For abbreviations, see list. Scale bar = 10 μm in E,G,H–O); 20 μm in D,F; 50 μm in R; 100 μm in A,B,P,Q.

either before or after crossing the midline. CPU1a cells innervating an ipsilateral CBU column cross the midline in the anterior chiasma, whereas cells innervating a contralateral column cross the midline in the posterior chiasma. The major neurite finally enters the contralateral isthmus tract and gives rise to an extensive arborization tree in the contralateral dorsal LAL (Fig. 9R). Neurons of this type have been found in most columns of the PB, indicating a set of 16 isomorphic cells with a heterolateral arborization scheme identical to that of *Drosophila* and locusts (Hanesch et al., 1989; Heinze and Homberg, 2008). A notable exception is the outermost PB column,

in which CPU1a neurons have not yet been labeled and remain hypothetical (Fig. 9C).

CPU1b neurons ($n = 4$) largely resemble CPU1a neurons (Fig. 9D–F). However, the primary neurite does not invade the ipsilateral PB, but, after bypassing the PB, crosses the midline in the posterior chiasma and sends off a major fiber that innervates the medialmost column of the contralateral PB. Thus, all arborization trees of CPU1b neurons are located in the contralateral brain hemisphere. The main neurite continues for a short distance along the posterior CBU surface, before innervating either the lateralmost two columns of the contralateral CBU hemisphere or the two columns medially adjacent to these. Finally, the main neurite enters the isthmus tract and projects toward the dorsal LAL. Here, it continues without branching to the anterior end of the LAL, turns by

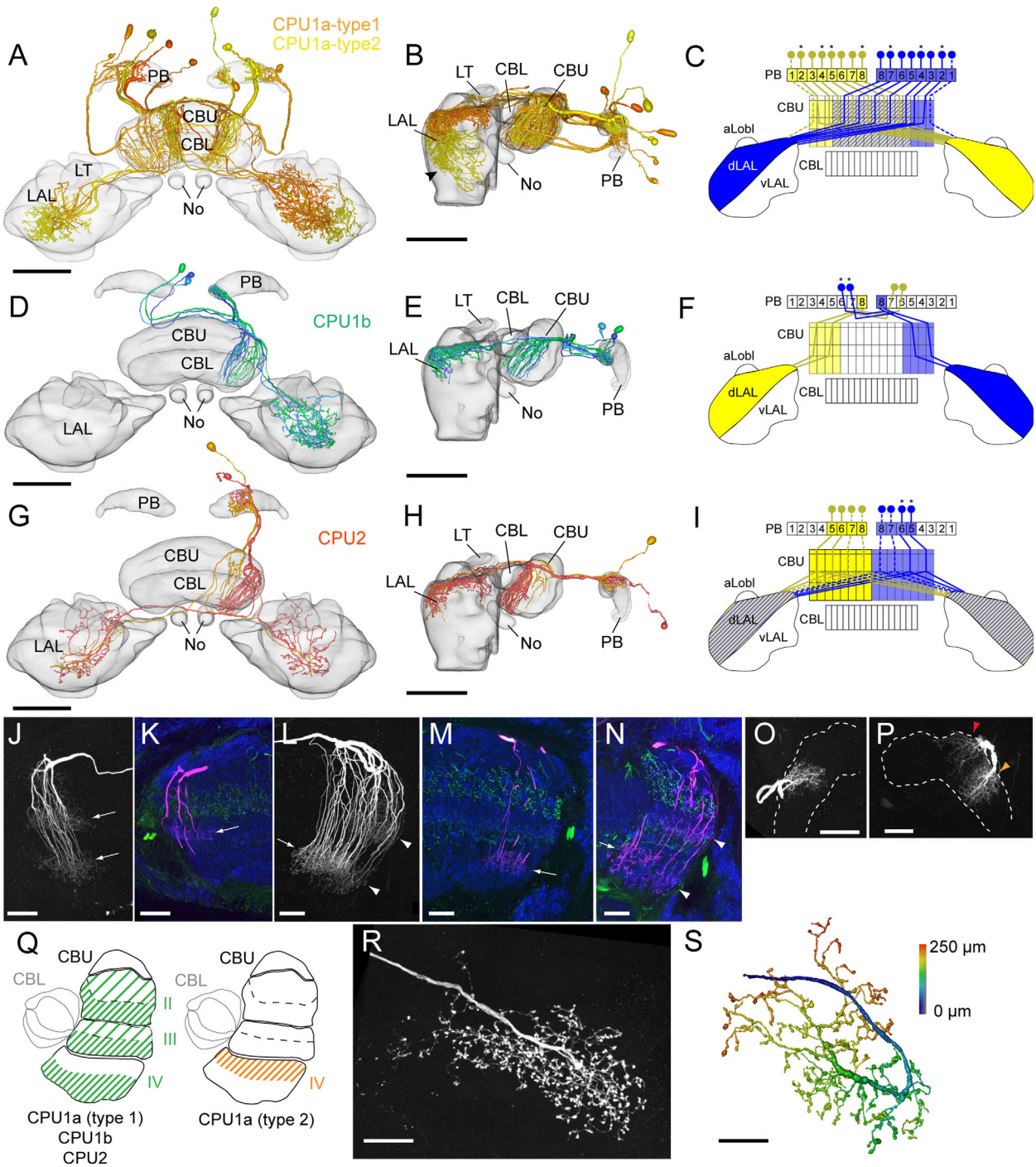

Figure 9

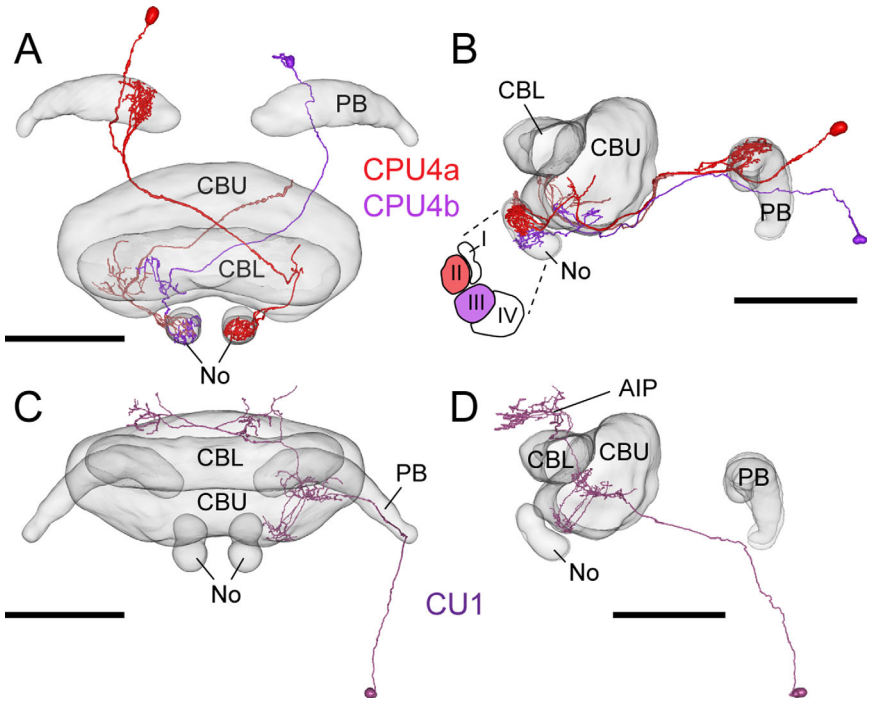

Figure 10. Additional types of columnar neurons of the CBU. **A/B**: 3D reconstruction of columnar neurons of the CBU that innervate the noduli (A, frontodorsal view; B, lateral view). PB projections could not be resolved in the CPU4b cell, and one CPU4a neuron could not be traced beyond the CBU. CBU arborizations in the second CPU4a cell are incomplete. The inset in B schematically illustrates the noduli layers innervated by CPU4a and CPU4b neurons. **C,D**: 3D reconstruction of a CU1 neuron providing bilateral output from the central body to the anterior inferior protocerebrum (AIP). C, frontal view; D, lateral view. For abbreviations, see list. Scale bar = 100 μm in A–D.

180°, and projects back toward the CBU while giving rise to widely branching arborizations with large beaded terminals (Fig. 9S). CPU1b neurons were only found in the medialmost PB column and, given that they innervate different sets of CBU columns, do not appear to constitute an isomorphic set of cells. Hence two individual CPU1b cells are likely unique for the medialmost PB column (Fig. 9F).

CPU2 neurons ($n = 2$) share most characteristics with CPU1a neurons (Fig. 9G–I). The major difference is the

Figure 9. Columnar output neurons of the CBU. **A,B**: 3D reconstructions of six CPU1a neurons registered into the standardized compass neuropils (A, frontodorsal view; B, lateral view). Note that not all neurons shown could be reconstructed to completeness due to weak or superimposed staining. The arrowhead in B indicates the LAL projections of CPU1a type 2 neurons, innervating further posterior regions of the LAL than CPU1a type 1 cells. **C**: Proposed heterolateral connectivity scheme of CPU1a neurons. Identified neurons are marked by an asterisk. The dashed neuron innervating the lateralmost column has not been identified and remains hypothetical (based on Hanesch et al., 1989). **D–F**: As A–C, but for three CPU1b neurons. These cells appear to exist only as two individual cells on either hemisphere (F). **G–I**: As A–C, but data are shown for two CPU2 neurons. As only two examples were found (asterisks in I) the heterolateral connectivity scheme remains largely hypothetical. However, the innervation of the lateralmost CBU column by a neuron originating in PB column R5 suggests that CPU2 cells do not exist in the lateral PB columns. **J**: Confocal image of CBU arborizations of a CPU1a neuron. Arrows indicate selective, dense innervation of certain CBU layers. **K**: Detail of preparation shown in J, illustrating the relation of innervated layers with respect to serotonin immunoreactivity (green). Synapsin immunoreactivity is shown in blue, and injected neuron is shown in magenta. The arrow highlights dense innervation of layer IIIb. **L**: Confocal image of a double injection of a CPU1a (type 2) and a CPU2 cell (arrowheads: dense arborizations of the CPU2 cell; arrow: dense fibers of the CPU1a type 2 cell). **M,N**: Details of arborization trees shown in L (colors as in K). M shows a posterior level of the image stack revealing fibers of the CPU1a type 2 cell (arrow), and N shows a more anterior level revealing fibers of the CPU2 cell as well (arrowhead). **O,P**: Confocal images of arborization trees in the PB; O, CPU1a type 1; P, CPU2 (red arrowhead), CPU1a type 2 (yellow arrowhead). **Q**: Schematic illustration of innervated CBU layers by the different types of CPU1/2 neurons. **R**: Confocal image of arborization tree in the LAL (CPU1a type 1 cell), revealing clearly beaded fiber terminals. **S**: Surface reconstruction of LAL arborizations of CPU1b neuron. The colors indicate distance from origin and highlight the finding that this cell type passes the LAL without branching, turns around at the anterior tip of the LAL, and sends fibers into the LAL from the opposite side of the other CPU1/2 neurons. Scale bar = 20 μm in J–P,R,S); 100 μm in A,B,D,E,G,H.

presence of an axon that bifurcates in the anterior chiasma and projects to both LALs. Second, the heterolateral arborization scheme appears to differ from that of CPU1 neurons. Although only two individual neurons have been found, the innervated columns suggest that these cells only exist in the four medial PB columns and connect these to one of four columnar segments, which together span the complete ipsilateral CBU hemisphere (Fig. 9I).

A detailed look at the columnar arborization domains in the CBU allowed more refined mapping of the proposed input arborizations of CPU1/2 neurons. By using anti-serotonin colabeling in rehydrated thick sections containing injected neurons, we established that terminals were not equally distributed across CBU layers. Emerging from the main neurite are thin, filamentous fibers that pass orthogonally through all CBU layers (Fig. 9J–N). From these, fine fibers spread laterally in layers II, IIIa, and the ventral part of layer IV. These fibers form a dense mesh of minute terminals in layers IIIa and ventral layer IV, whereas layer II is less densely innervated. Laterally, these arborization domains cover about one-eighth of the width of the CBU. This innervation pattern has been found in CPU1a, CPU1b, and CPU2 neurons. However, three examples of CPU1a cells possessed a different morphology (Fig. 9L,M,Q). Even though they shared all other features with the remaining CPU1a neurons, fine terminals were only present in the dorsal part of layer IV, a region spared by the other cell types. Interestingly, the innervated region of the dorsal LAL also differed from all remaining cells, and extended further ventral and posterior (Fig. 9B). Thus, these neurons likely constitute a distinct subtype of CPU1a cells and were termed *type 2* (as opposed to *type 1* for the remaining CPU1a neurons). The LAL arborizations in the remaining neurons (CPU1a type 1, CPU1b, CPU2) showed complete overlap and appeared to innervate microglomerular domains of identical regions in the dorsal LAL.

The remaining three types of CBU columnar neurons were found less frequently (Fig. 10). The first type innervated the PB, the CBU, and the contralateral nodulus, and was termed a CPU4 neuron (according to Heinze and Homberg, 2008). It was found in three examples, one of which could not be traced to the PB, whereas PB arborizations of another one could not be resolved (Fig. 10A,B). Originating from the somata, their primary neurites projected to a medial PB column, crossed the midline in the posterior chiasma, and sent a few arborizations into CBU layer IV and to layer II (CPU4a) or III (CPU4b) of the contralateral nodulus. The neuron projecting to No layer III innervated a more ventral region of CBU layer IV, suggesting a selective connection between CBU layers and No layers (Fig. 10B). In all examples, terminals in the CBU appeared beaded, whereas the appearance of the remaining arborization trees did not indicate a clear polarity of the cells. The last type of neuron was termed a CU1 neuron ($n = 3$) (Heinze and Homberg, 2008) and connects a columnar arborization domain of the CBU with bilateral regions in the AIP (Fig. 10C,D). The primary neurites project toward the PB and continue to the posterior CBU surface. Here, they either cross the midline to innervate a contralateral CBU column, or they directly innervate an ipsilateral CBU column. The primary neurite enters the CBU ventrally or laterally and projects to layer IIIb, where it gives rise to a mesh of fibers filling approximately one-eighth of the CBU width. Fine fibers protrude ventrally from these arborizations and form a second arborization tree at the ventral extreme of layer IV. Additionally, one major fiber branches off the arborizations in layer IIIb and projects anteriorly. After passing through the CBL, it bends medially and sends off branches that form a loose mesh of beaded terminals in bilaterally symmetrical regions of the AIP, just anteriodorsal to the CBL.

DISCUSSION

In the monarch butterfly, neurons in a group of neuropils in the central brain have been shown to respond to skylight compass cues (Heinze and Reppert, 2011). Together with data from the desert locust (Homberg et al., 2011), this indicates that these regions are the neural substrate of an internal sun compass and were thus termed sun compass neuropils. They comprise the CX, the LAL, and the AOTu. To aid further functional analysis, we established a standardized, average-shape representation of these regions. This standardized compass neuropil was used as a volumetric reference and as a tool to register numerous neurons into a common frame of reference.

Volumetric differences between migrants and nonmigrants

We tested whether the standard neuropil volumes could be used as a reference for intraspecific comparisons. In general, larger neuropil volumes have previously been associated with increased processing power due to higher numbers of synapses. For example, in honey bees, the volume of the mushroom bodies increases after a worker bee transitions from nursing bee to forager, correlating with increased sensory input and an increased requirement for navigational tasks (Farris et al., 2001; Ismail et al., 2006; Groh et al., 2012). Thus, we examined whether it would be possible to extract meaningful information from comparisons of volumetric data obtained from monarchs differing in their behavioral states.

This comparison showed that the relative volume of the PB was significantly increased only in animals with extensive migratory experience. This is consistent with previous findings in locusts suggesting that the PB

houses a 360° map of azimuthal space and thus would be of crucial importance during long-distance migration (Heinze and Homberg, 2007). Recordings from neurons of the monarch PB also showed responses to skylight compass cues, and their function is thus consistent with this expectation (Heinze and Reppert, 2011). The fact that a similar, albeit not significant, trend toward increased volume in experienced migrants has been found for the CBL (a neuropil most tightly connected with the PB), whereas no unambiguous trend was seen for the CBU (which is assumed to encode nonspatial sensory information), underscores our finding that the detected changes in relative volume indeed match expectations and suggests that they contain predictive value with regard to neuropil function.

The smaller relative volumes of the components of the AOTu, in particular the large upper unit, might indicate that the more stereotypical behavior during the later stages of migration requires less processing of visual information in comparison with the territorial foraging of summer monarchs or the fuel foraging of early migrants. As the AOTu is a relay station for visual information from the optic lobe (Pfeiffer et al., 2005; Kinoshita et al., 2007; Mota et al., 2011), its volume could be indicative of the amount of preprocessing necessary to extract behaviorally relevant information represented in the central brain. This is consistent with findings comparing solitary phase locusts and gregarious, migratory locusts (Ott and Rogers, 2010). In the locust, peripheral neuropils such as the optic lobes and the antennal lobes are reduced in relative size in the migratory gregarious state, whereas more central, higher order neuropils are increased in size. Interestingly, the absolute volume of the brains of migratory locusts is also substantially increased, a finding virtually identical to the age-dependent size increase found in migratory monarchs.

Generally, the differences between neuropil volumes from different groups of monarchs and the standard neuropil volumes match known findings. They are also consistent with results from other species and are useful for making functional predictions about less well understood brain regions. Comparisons with the standard neuropil volumes can help pinpoint brain regions involved in a particular behavior. Likewise, such comparison can ultimately guide more detailed analysis aimed at the underlying mechanisms of the volume changes and their links to specific aspects of a behavioral strategy.

The standardized compass neuropils as common frame of reference

In the current work, we were able to register more than 55 individual neurons of 34 distinct cell types into the common frame of reference provided by the standardized sun compass neuropils. Thus, conclusions can be drawn about overlapping projection patterns of different neurons, about the layout of heterolateral connectivity schemes, and about compartmentation of brain regions not easily recognizable based on immunostaining alone. Projection patterns resulting from registration of neurons were validated by rehydration and double labeling of these cells, showing that the relative location of arborizations with respect to neuropil boundaries is preserved during the standardization procedure. Because of the large number of neurons registered into the standard, we were able to identify some limitations of the registration process more clearly than in previous uses of this method (Brandt et al, 2005; el Jundi et al, 2010; Løfaldli et al, 2010; see Materials and Methods for details). However, these limitations did not affect the overall layout and shape of neuron types and their projection areas—the major aim of the current work.

Segregation of input pathways into the central body

The source of information reaching the CX is of vital importance for understanding the integrative role this structure plays in its proposed functions as an internal compass as well as a center for visual learning and multimodal information processing. Input to the CX is generally thought to be mediated through tangential neurons innervating one of the subunits of the central body, and, to a lesser extent, the PB and the noduli. The polarity of these neurons is largely inferred from the appearance of terminals, in which varicose endings indicate output sites and smooth endings indicate input sites (Hanesch et al., 1989; el Jundi et al., 2010). Recent work in *Drosophila* has confirmed this polarity by expressing pre- and postsynaptic markers in Gal4 driver lines targeting CBU tangential neurons (Li et al., 2009; Young and Armstrong, 2010). In all neurons examined, presynaptic markers are found only in the CBU, not in extrinsic arborization areas. Additionally, electron microscopy in the desert locust has revealed postsynaptic sites in γ-aminobutyric acid (GABA)-immunoreactive neurons of the LT, which very likely represent dendrites of CBL tangential neurons (Träger et al., 2008).

Proposed input neurons of the CBL and the CBU receive information from largely non-overlapping regions of the central brain (Fig. 11). Although they are relatively uncharacterized in the monarch butterfly, comparison with other insects suggests that all of these regions are not directly involved in primary sensory processing, but appear to be higher order relay stations. The greatest variety of inputs serves distinct layers of the CBU and originates from the superior protocerebrum, the inferior

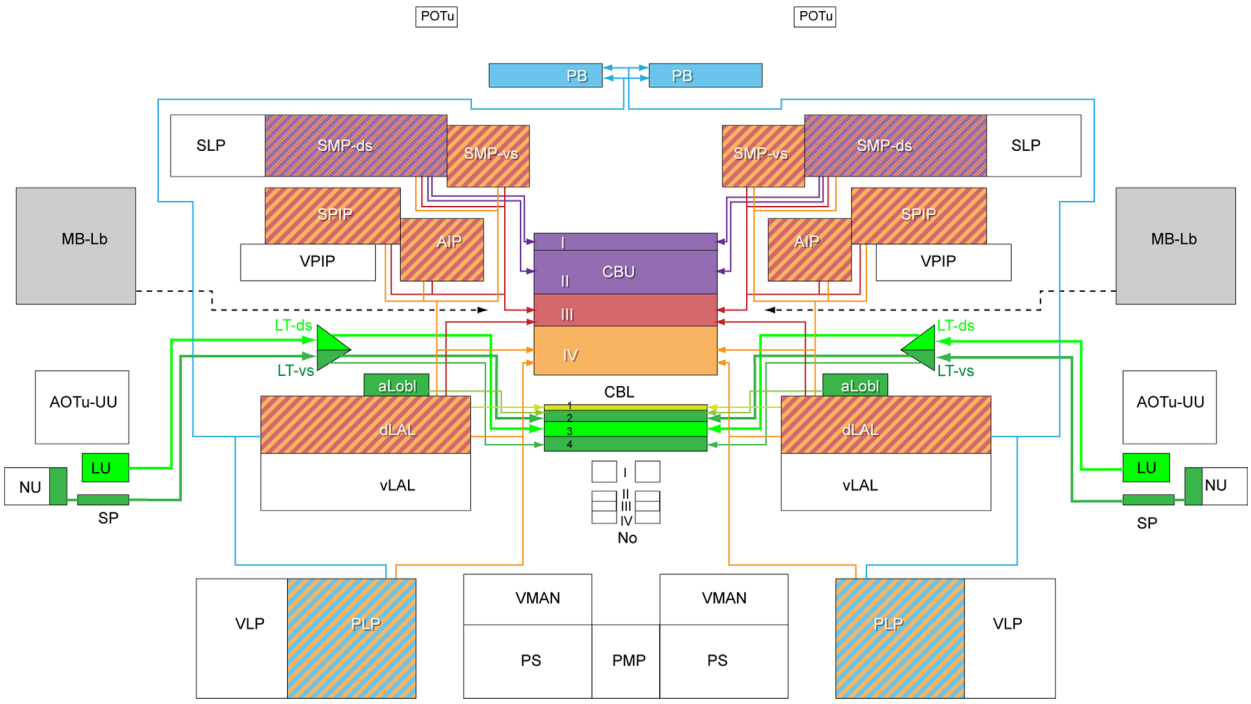

Figure 11. Summary of input pathways to the central complex. Schematic representation of components of the monarch central brain and their connections to the central complex (CX), illustrating the segregation of inputs to the upper and lower divisions of the central body. Regions connected to components of the CX are highlighted in the respective color. Regions providing input to more than one layer/parts of the CX are hatched. Identified neural connections are indicated as arrows. As the connection from the mushroom body lobes could not be traced to any particular layer of the central body, it is depicted as dotted line. SLP, superior lateral protocerebrum; SMP-vs, ventral shell of superior medial protocerebrum; SMP-ds, dorsal shell of superior medial protocerebrum; SPIP, superior posterior inferior protocerebrum; VPIP, ventral posterior inferior protocerebrum; AIP, anterior inferior protocerebrum; VLP, ventrolateral protocerebrum; PLP, posterior lateral protocerebrum; VMAN, ventromedial anterior neuropils; PS, posterior slope; PMP, posterior medial protocerebrum.

protocerebrum, the dorsal LAL, and the PLP (for definitions of these terms, see Heinze and Reppert, 2012). No systematic mapping of input regions to specific CBU layers was observed, and identical layers received input from multiple brain regions. This layout is thus well suited to implement convergence of a multitude of highly processed pieces of information. The proposed input regions, particularly in the superior protocerebrum, as well as the shape and fiber trajectories of several TU neurons, match up well with known fan-shaped neurons from *Drosophila* (Hanesch et al., 1989; Li et al., 2009; Young and Armstrong, 2010) and the flesh fly *Neobellieria bullata* (Phillips-Portillo and Strausfeld, 2012).

Such neurons innervating the superior protocerebrum have been implicated in memory processing of specific visual features in *Drosophila* (Liu et al., 2006; Wang et al., 2008). Neural connections to the CBU originating in the PLP and the LAL also suggest that visual information is relayed to the CBU layers, as work in other species has shown that these regions are targeted by projection neurons from the optic lobes either directly (PLP; Rind, 1987; Otsuna and Ito, 2006; Strausfeld and Okamura, 2007; Paulk et al., 2009) or indirectly (LAL; Pfeiffer et al., 2005).

Unlike the CBU, all neurons targeting the CBL originate from the LAL, in particular from the LT. Projections from the LT could be allocated to one of two pathways (Fig. 11). The first pathway originates in the lower unit of the AOTu, passes through the dorsoposterior sector of the LT, and ends in layer 3 of the CBL (TuLAL1b and TL3 neurons). The second pathway originates in the strap of the AOTu, passes through the ventroanterior sector of the LT, and ends in layers 2 and 4 of the CBL (TuLAL1a and TL2 neurons). The fact that no neurons have been found innervating the ventromedial sector of the LT and most parts of the nodular unit of the AOTu suggests the existence of a third pathway specifically connecting these two compartments. Neurons within both clearly identified pathways are tuned to the *E*-vector orientation of polarized light, as well as to the azimuth position of unpolarized light and thus carry information about skylight compass cues (Heinze and Reppert, 2011). Interestingly, two parallel input pathways to the CBL also exist in the

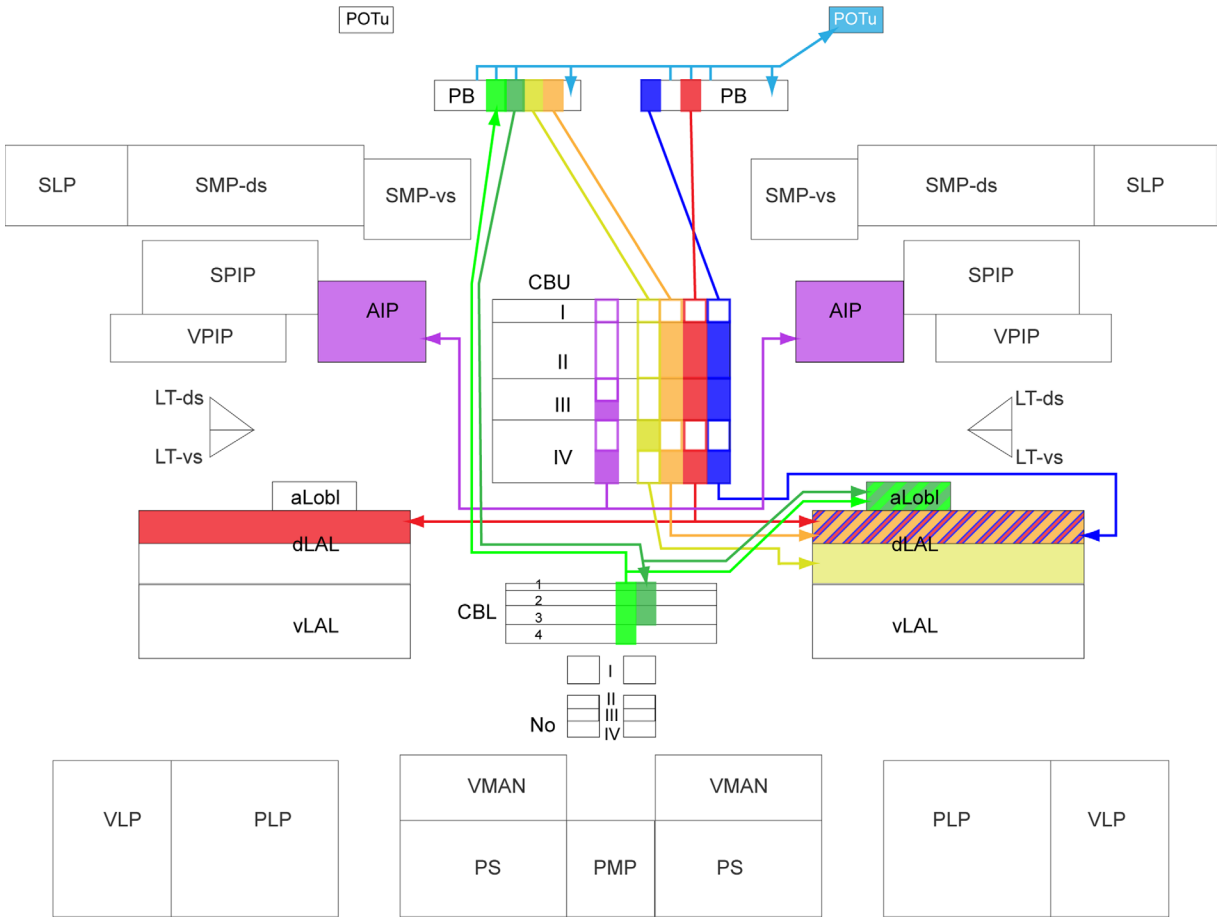

Figure 12. Summary of output pathways from the central complex. Schematic representation of components of the monarch central complex and their connections to regions of the central brain. Output pathways are represented by individual neuron types and shown only for the left hemisphere (bilateral output neurons are shown on both sides of the midline). Regions served by a particular neuron are highlighted in the respective color. Note that for better visibility isomorphic sets of columnar cells are depicted as individual cells only. Layers of the central body from which neurons receive input are indicated by filled rectangles, and layers without fibers are left empty. Abbreviations as in legend of Figure 11.

polarization-sensitive network of the locust (Träger et al., 2008; Heinze et al., 2009; Homberg et al., 2011).

The first one projects from the lower unit of the AOTu and the anterior lobula to the LT and medial olive of the LAL (TuLAL1b neurons), and further on to layer 5 of the CBL (TL3 neurons). The second pathway projects from the lower unit of the AOTu to the LT (TuLAL1a neurons), and further on to layer 2 of the CBL (TL2 neurons). In the locust, TL2 neurons have been shown to carry *E*-vector information from both eyes, whereas TL3 neurons only receive monocular input (Vitzthum et al., 2002; Heinze et al., 2009). The functional significance of these dual input pathways, both involved in sun compass navigation, remains unclear. However, as they appear to be highly conserved and do not carry identical information, their combined presence is likely important for providing proper input to the CX compass network.

Convergence of information onto downstream targets of the central complex

To illuminate the role of the CX in motor control and to understand how compass information in this structure is used to guide behavior, we examined the possible output pathways from the CX (Fig. 12). As for input pathways, morphological features of arborizations (presence of varicosities) have been used to infer the polarity of output neurons. Unlike the proposed input pathways, which originate in a great variety of brain areas, the proposed output cells target almost exclusively compartments of the LALs. The only exceptions from this were CU1 neurons connecting CBU columns to small, bilateral regions of the AIP, and TB1 neurons, which possess a collateral branch innervating the posterior optic tubercle. Interestingly, the morphology of CU1 neurons resembled that of locust neurons innervating the anterior lip, a CX-associated neuropil, whose counterpart in other insects has

remained elusive (Heinze and Homberg, 2008; el Jundi et al., 2010). Based on the morphology of CU1 neurons, our data suggest that the anterior lip is a specialization of the AIP.

All remaining potential output cells are columnar neurons of the PB with additional arborizations in either the CBU (CPU1/2 neurons) or the CBL (CL1 neurons). The output regions of CPU1a, CPU1b, and CPU2 neurons show complete overlap in regions of the dorsal LAL, the only exception being CPU1a type 2 neurons, which project to further posterior and ventral regions of the dorsal LAL. Interestingly, these neurons also differed in the innervated CBU layers, suggesting that information from specific CBU layers is transferred to individual subdomains of the dorsal LAL. The CPU1a, CPU1b, and CPU2 neurons have all been described previously in the locust. Their monarch counterparts reflect the morphology of these locust cells in remarkable detail. The most striking difference, however, is that the locust cells project to the ventral shell of the LAL (Heinze and Homberg, 2008), suggesting that the dorsal LAL of the monarch is homologous to the ventral shell of the locust LAL, contrary to what had been inferred from projection patterns of serotonergic neurons (Heinze and Reppert, 2012). When the details of LAL projections in the monarch neurons are examined, the terminal varicosities are seen to be concentrated in microglomerular domains, typical of the dorsal LAL (Heinze and Reppert, 2012). These regions of increased synaptic density thus appear to be the convergence site for multiple CPU1/2 neurons. Whether the different subtypes with overlapping projection areas innervate distinct or overlapping sets of microglomeruli remains to be shown. In this context, it is noteworthy that CPU1b neurons innervate the LAL from the opposite direction compared with the remaining cell types. This suggests that the precise timing of output and the possibly synchronous convergence of CPU1a/2 and CPU1b neurons in a defined set of LAL microglomeruli could both be important for relaying information from the CX to downstream neurons.

Columnar neurons with arborizations in the CBL (CL1 neurons) possess axonal projections converging in one small region of the LAL, the newly defined anterior loblet (Heinze and Reppert, 2012). Interestingly, both subtypes appear to avoid the pronounced microglomeruli of this region and to target regions of low synaptic density. Although the functional significance of this finding remains unclear, it could suggest that nonsynaptic volume transmission plays a major role in relaying information to postsynaptic cells. Consistent with this possibility is the presence of neuropeptides in homologous cells in the locust (Vitzthum and Homberg, 1998). The corresponding neurons in the locust have been reported to project to the LT (Müller et al., 1997; Heinze and Homberg, 2008). However, their projections appear not to enter the GABAergic part of the LT, but rather fill a spherical layer enclosing this structure from all sides (S. Heinze, unpublished observation). Compared with the monarch, CL1 neuron arborizations in the locust LAL are much smaller in their extent as well as fiber diameter, suggesting that this output pathway plays a more important role in the monarch brain.

Defining the core components of the central complex

To draw conclusions about the general function of the CX, as well as its specific role in guiding migratory behavior in the monarch butterfly, we identified its core components, i.e., the neuronal elements conserved across a wide variety of insects. These fundamentally shared elements likely provide the substrate for the key computations performed by this midline structure. Understanding these processes will ultimately explain how this brain region is implicated in such diverse aspects as visual pattern learning, the coordination of locomotion, and the processing of polarized light.

Detailed catalogues of CX neurons have been obtained for *Drosophila* (Hanesch et al., 1989) and the desert locust (Heinze and Homberg, 2008), whereas isolated neuron morphologies have been reported in the honey bee (Homberg, 1985), the beetle *Tenebrio* (Wegerhoff et al., 1996), crickets (Schildberger, 1983; Sakura et al., 2008), several larger fly species (Strausfeld, 1976; Phillips-Portillo and Strausfeld, 2012; Phillips-Portillo, 2012), and the monarch butterfly (Heinze and Reppert, 2011). When comparing these earlier results with our new monarch dataset, it becomes apparent that neuronal cell types of the PB and the CBL are highly conserved across species. Although comparisons with the CBL of flies (ellipsoid body) are more difficult due to its toroid shape and the resulting distortions of layers into concentric rings (Young and Armstrong, 2010), the fly's R neurons are clearly homologous to the monarch TL neurons. As the locust CBL resembles that of the monarch more closely, we were able to identify locust counterparts of all five types of monarch TL neurons, based on the location of input and output arborizations and physiological responses to skylight compass cues (Müller et al., 1997; Vitzthum et al., 2002; Heinze and Reppert, 2011). Only one type of locust TL neuron (TL5; likely a dopaminergic modulatory neuron; Wendt and Homberg, 1992; Vitzthum et al., 2002) was not detected in the monarch. The large overlap of TL neurons between the locust and the monarch suggests that a comprehensive neuronal set has been identified that defines the major input elements of the insect CBL.

Equally striking were the similarities of intrinsic PB neurons (TB1) and columnar neurons (CL1/2, CPU1/2/4), for which locust counterparts could be identified for all nine monarch cell types. TB1 neurons were virtually identical between the monarch and the locust with respect to innervation patterns and the structure of arborization trees (Heinze and Homberg, 2007). Similar, albeit less well described, TB1-like neurons have also been reported in bees (Homberg, 1985) and *Drosophila* (Hanesch et al., 1989; Young and Armstrong, 2010), and indicate that the complex interhemispheric information flow, suggested by the unique morphology of these cells, is a fundamental feature of the insect PB.

Columnar neurons of the CBL (CL1/2 neurons) were also conserved on multiple levels. For CL1 neurons, the monarch cells represented their locust homologues with respect to gross morphology, structure of input and output regions, presence of subtypes with opposite polarity, and a heterolateral connectivity scheme (Heinze and Homberg, 2008). The opposite polarity of CL1a/b neurons suggests that the direction of information flow between the CBL and the PB is opposite between the two CL1 subtypes. This is consistent with data from the desert locust (Heinze and Homberg, 2008, 2009) and *Drosophila* (Hanesch et al., 1989). Importantly, CL1a neurons are the only columnar cells found to date that appear to have their output to the PB and could therefore provide a link between CBL input neurons and neurons with input areas in the PB. Based on physiological response characteristics to polarized light, information flow from the CBL to the PB has been proposed as one of the key features of the CX compass network in the locust (Heinze et al., 2009). Altogether, the conservation of these neurons indicates that bidirectional information flow between the PB and the CBL is an important feature of the insect CX.

Columnar neurons of the CBU were also highly conserved between the monarch and the locust. In fact, CPU1 cells closely resembled each other with respect to the structure of arborization trees, neuron polarity, and heterolateral connectivity schemes (Heinze and Homberg, 2008). Although input-like fibers were found in the PB and CBU of both species, the CBU layers targeted by these fibers differed substantially, indicating species-specific differences in the information transmitted to these neurons. Importantly, neurons of highly similar morphology have also been described in bees and flies (Homberg, 1985; Hanesch et al., 1989; Phillips-Portillo, 2012). Their widespread occurrence, uniquely pronounced polarity, and large neurite diameter underscore that these cell types likely constitute the major output pathway of the insect CX. The addition of recent physiological data (Heinze and Reppert, 2011) bolsters the idea that a network involved in the processing of skylight compass cues and the generation of an internal representation of azimuthal space (consisting of TL2/3, CL1, TB1, and CPU1 cells) is present in all insects and might represent the core computational elements that define CX function.

Contrary to CBL/PB neurons, our data indicate more variability among insect species within the population of cells exclusively associated with the CBU. With the exception of neurons connecting the superior protocerebrum to dorsal CBU layers, which have also been described in flies (Li et al., 2009; Young and Armstrong, 2010; Phillips-Portillo and Strausfeld, 2012), no counterparts of CBU input neurons from other species could be identified (Schildberger, 1983; Homberg, 1985; Hanesch et al., 1989; Müller et al., 1997; Homberg et al., 1999; el Jundi et al., 2010). This might be the result of the existence of a large pool of cell types, of which only a small fraction has been identified in each species, or because neurons show specialized morphologies in individual species. The fact that we identified all types of TU cells only as individual examples suggests that there are indeed many different morphological types, a conclusion shared by the authors of earlier studies (Hanesch et al., 1989). Another factor is the potentially variable shape of the regions providing input to TU neurons in different species. Moreover, these regions, usually referred to as "unstructured neuropils," are largely uncharted in most insects, and attempts to define them more rigorously have been made only in *Drosophila* (Otsuna and Ito, 2006) and the monarch (Heinze and Reppert, 2012). Hence, comparative studies are at an early stage regarding this vast group of neurons.

Nevertheless, the trend toward species-specific specializations in the CBU, which would complement the highly conserved core CBL/PB network described, is supported by the specialization already described in the CBU-associated fibers of monarch CPU1/2 cells. In addition, of the three identified pontine cell types of the CBU, only PoU3 cells have a clear counterpart in the locust, whereas the others differ in the specific layer they innervate (Heinze and Homberg, 2008). Although TU neurons and pontine cells have been identified in all insects examined and generally follow a similar ground pattern of arborizations (Homberg, 1985; Hanesch et al., 1989; Siegl et al., 2009; Phillips-Portillo, 2012), the detailed locations of their arborization trees appear to be species-dependent, suggesting functional differences in the information flow to and between CBU layers. This is consistent with data from flies that implicate the CBU in memory for selective, behaviorally relevant visual stimuli (Liu et al., 2006; Pan et al., 2009), as the lifestyle of each species likely determines which features of the environment are behaviorally relevant. Species-specific differences in CBU-associated information flow would thus be expected. However, it remains possible that most of the

CBU-associated neurons could be homologous across insects and only differ in their shape between species because of the gross differences in neuropil structure (arrangement of layers, etc). Thus, physiological studies across insect species are required to resolve whether CBU neurons are functionally homologous and encode similar information in all insects. Alternatively, these cells may be involved in species-specific encoding of behaviorally relevant information and thus contribute to conferring the unique behavioral identity of each species.

Toward a functional map of central-complex circuits

To ultimately understand the role of the CX in guiding monarch butterfly navigation, a functional map of its neuronal circuitry is needed. Such a circuit map will facilitate our understanding of how the inputs that reach this structure are processed and transformed into output signals, which can then be used to produce motor commands. Our analyses, enabled by the standardized compass neuropils of the monarch, provide the foundation for a connectivity map by narrowing down the neuronal inputs, defining the output pathways, and obtaining information about circuit elements within the CX. These circuit elements comprise parallel input pathways, systematic interhemispheric connectivity patterns, and multiple potential feedback loops. These feedback loops are particularly prominent within the recurrent connections between the CBL and PB, but are also possible between the CBL and the anterior loblet of the LAL, and between the CBU and the dorsal LAL. These individual components can now be linked on the basis of overlapping arborization trees and used as a basis for modeling efforts and for functional or electron microscopic verification of synaptic connections. As all neurons are registered into the same frame of reference, aspects of their morphology can be quantified and directly compared with each other. Therefore, realistic circuit models that take the anatomical features of neurons into account are feasible. Importantly, newly registered neurons can be added to the dataset presented, and thus an increasingly comprehensive set of circuit elements will emerge over time.

Overall, our data suggest that effort should be directed toward unraveling the synaptic connectivity between the conserved neurons of the CX core network, so that realistic models of the basic computations performed by this brain region can be developed. Combined with additional functional analysis of the key elements identified in this study, we hope that this anatomical framework will lead to a fuller understanding of the neural processes underlying migratory behavior in the monarch butterfly. This framework will probably also increase our understanding of general CX function in insects and perhaps illuminate fundamental mechanisms of sensorimotor transformation in all animals.

ROLE OF AUTHORS

All authors had full access to all the data in the study and take responsibility for the integrity of the data and the accuracy of the data analysis. Study concept and design: S.H., S.R. Data acquisition: S.H., S.A., J.F. Analysis and interpretation of data: S.H., J.F., S.A., B.J., S.R. Standardization of neuropils: B.J. Drafting of the manuscript: S.H. Critical revision of the manuscript for important intellectual content: S.R., B.J. Obtained funding: S.H., S.R. Study supervision: S.H., S.R.

ACKNOWLEDGMENT

We thank Torsten Rohlfing for technical assistance with standardization and for providing the ISA tools. The registration tools used are part of the Computational Morphometry Toolkit (CMTK), which is available at http://nitrc.org/projects/cmtk/. We are grateful to the Homberg laboratory and the HRZ at the University of Marburg for providing access to a Linux cluster for standardization; Jan-Felix Evers for providing an updated version of the Amira skeletonize tool; Harlen E. Aschen, Altus Aschen, Carol Cullar, David G. Cook, and Fred Gagnon for butterflies; Lauren Beaver, Lauren Foley, Daniel Newman, and Andy Dowd for butterfly husbandry; James Ashley for help with confocal microscopy; and the Budnik laboratory at the University of Massachusetts Medical School for allowing access to their Zeiss-LSM7 confocal microscope. We are also grateful to James Phillips-Portillo for providing three morphologies of CPU1 neurons, Uwe Homberg for helpful discussion on tangential cell nomenclature, and the Reppert laboratory for helpful discussions throughout the experiments.

CONFLICT OF INTEREST STATEMENT

The authors declare that they have no conflict of interest.

LITERATURE CITED

Bender JA, Pollack AJ, Ritzmann RE. 2010. Neural activity in the central complex of the insect brain is linked to locomotor changes. Curr Biol 20:921–926.

Brandt R, Rohlfing T, Rybak J, Krofczik S, Maye A, Westerhoff M, Hege H-C, Menzel R. 2005. Three-dimensional average-shape atlas of the honeybee brain and its applications. J Comp Neurol 492:1–19.

Dreyer D, Vitt H, Dippel S, Goetz B, el Jundi B, Kollmann M, Huetteroth W, Schachtner J. 2010. 3D standard brain of the red flour beetle *Tribolium castaneum*: a tool to study metamorphic development and adult plasticity. Front Syst Neurosci 4:3.

el Jundi B, Huetteroth W, Kurylas AE, Schachtner J. 2009. Anisometric brain dimorphism revisited: implementation of a

volumetric 3D standard brain in *Manduca sexta*. J Comp Neurol 517:210–225.

el Jundi B, Heinze S, Lenschow C, Kurylas AE, Rohlfing T, Homberg U. 2010. The locust standard brain: a 3D standard of the central complex as a platform for neural network analysis. Front Syst Neurosci 3:21.

Evers JF, Schmitt S, Sibila M, Duch C. 2005. Progress in functional neuroanatomy: precise automatic geometric reconstruction of neuronal morphology from confocal image stacks. J Neurophysiol 93:2331.

Farris SM, Robinson GE, Fahrbach SE. 2001. Experience- and age-related outgrowth of intrinsic neurons in the mushroom bodies of the adult worker honeybee. J Neurosci 21: 6395–6404.

Groh C, Lu Z, Meinertzhagen IA, Rössler W. 2012. Age-related plasticity in the synaptic ultrastructure of neurons in the mushroom body calyx of the adult honeybee *Apis mellifera*. J Comp Neurol 520:3509–3527.

Hanesch U, Fischbach KF, Heisenberg M. 1989. Neuronal architecture of the central complex in *Drosophila melanogaster*. Cell Tissue Res 257:343–366.

Heinze S, Homberg U. 2007. Maplike representation of celestial *E*-vector orientations in the brain of an insect. Science 315:995–997.

Heinze S, Homberg U. 2008. Neuroarchitecture of the central complex of the desert locust: intrinsic and columnar neurons. J Comp Neurol 511:454–478.

Heinze S, Homberg U. 2009. Linking the input to the output: new sets of neurons complement the polarization vision network in the locust central complex. J Neurosci 29: 4911–4921.

Heinze S, Reppert SM. 2011. Sun compass integration of skylight cues in migratory monarch butterflies. Neuron 69: 345–358.

Heinze S, Reppert SM. 2012. Anatomical basis of sun compass navigation I: The general layout of the monarch butterfly brain. J Comp Neurol 520:1599–1628.

Heinze S, Gotthardt S, Homberg U. 2009. Transformation of polarized light information in the central complex of the locust. J Neurosci 29:11783–11793.

Homberg U. 1985. Interneurones of the central complex in the bee brain (*Apis mellifera*, L.). J Insect Physiol 31: 251–264.

Homberg U. 1994. Flight-correlated activity changes in neurons of the lateral accessory lobes in the brain of the locust *Schistocerca gregaria*. J Comp Physiol A 175:597–610.

Homberg U. 2008. Evolution of the central complex in the arthropod brain with respect to the visual system. Arthropod Struct Dev 37:347–362.

Homberg U, Vitzthum H, Müller M, Binkle U. 1999. Immunocytochemistry of GABA in the central complex of the locust *Schistocerca gregaria*: identification of immunoreactive neurons and colocalization with neuropeptides. J Comp Neurol 409:495–507.

Homberg U, Hofer S, Pfeiffer K, Gebhardt S. 2003. Organization and neural connections of the anterior optic tubercle in the brain of the locust, *Schistocerca gregaria*. J Comp Neurol 462:415–430.

Homberg U, Heinze S, Pfeiffer K, Kinoshita M, el Jundi B. 2011. Central neural coding of sky polarization in insects. Philos Trans R Soc Lond B Biol Sci 366:680–687.

Ismail N, Robinson GE, Fahrbach SE. 2006. Stimulation of muscarinic receptors mimics experience-dependent plasticity in the honey bee brain. Proc Natl Acad Sci U S A 103: 207–211.

King JR, Christensen, TA, Hildebrand JG. 2000. Response characteristics of an identified, sexually dimorphic olfactory glomerulus. J Neurosci 20:2391–2399.

Kinoshita M, Pfeiffer K, Homberg U. 2007. Spectral properties of identified polarized-light sensitive interneurons in the brain of the desert locust *Schistocerca gregaria*. J Exp Biol 210:1350–1361.

Klagges BR, Heimbeck G, Godenschwege TA, Hofbauer A, Pflugfelder GO, Reifegerste R, Reisch D, Schaupp M, Buchner S, Buchner E. 1996. Invertebrate synapsins: a single gene codes for several isoforms in *Drosophila*. J Neurosci 16:3154–3165.

Kurylas AE, Rohlfing T, Krofczik S, Jenett A, Homberg U. 2008. Standardized atlas of the brain of the desert locust, *Schistocerca gregaria*. Cell Tissue Res 333:125–145.

Kvello P, Løfaldli BB, Rybak J, Menzel R, Mustaparta H. 2009. Digital, three-dimensional average shaped atlas of the *Heliothis virescens* brain with integrated gustatory and olfactory neurons. Front Syst Neurosci 3:14.

Li W, Pan Y, Wang Z, Gong H, Gong Z, Liu L. 2009. Morphological characterization of single fan-shaped body neurons in *Drosophila melanogaster*. Cell Tissue Res 336:509–519.

Liu G, Seiler H, Wen A, Zars T, Ito K, Wolf R, Heisenberg M, Liu L. 2006. Distinct memory traces for two visual features in the *Drosophila* brain. Nature 439:551–556.

Løfaldli BB, Kvello P, Mustaparta H. 2010. Integration of the antennal lobe glomeruli and three projection neurons in the standard brain atlas of the moth *Heliothis virescens*. Front Syst Neurosci 4:5.

Merlin C, Gegear RJ, Reppert SM. 2009. Antennal circadian clocks coordinate sun compass orientation in migratory monarch butterflies. Science 325:1700–1704.

Mota T, Yamagata N, Giurfa M, Gronenberg W, Sandoz JC. 2011. Neural organization and visual processing in the anterior optic tubercle of the honeybee brain. J Neurosci 31: 11443–11456.

Müller M, Homberg U, Kühn A. 1997. Neuroarchitecture of the lower division of the central body in the brain of the locust (*Schistocerca gregaria*). Cell Tissue Res 288:159–176.

Neuser K, Triphan T, Mronz M, Poeck B, Strauss R. 2008. Analysis of a spatial orientation memory in *Drosophila*. Nature 453:1244–1247.

Otsuna H, Ito K. 2006. Systematic analysis of the visual projection neurons of *Drosophila melanogaster*. I. Lobula-specific pathways. J Comp Neurol 497:928–958.

Ott SR. 2008. Confocal microscopy in large insect brains: zinc-formaldehyde fixation improves synapsin immunostaining and preservation of morphology in whole-mounts. J Neurosci Methods 172:220–230.

Ott SR, Rogers SM. 2010. Gregarious desert locusts have substantially larger brains with altered proportions compared with the solitarious phase. Proc Biol Sci 277:3087–3096.

Pan Y, Zhou Y, Guo C, Gong H, Gong Z, Liu L. 2009. Differential roles of the fan-shaped body and the ellipsoid body in *Drosophila* visual pattern memory. Learn Mem 16: 289–295.

Paulk AC, Dacks AM, Phillips-Portillo J, Fellous J-M, Gronenberg W. 2009. Visual processing in the central bee brain. J Neurosci 29:9987–9999.

Pfeiffer K, Kinoshita M. 2012. Segregation of visual inputs from different regions of the compound eye in two parallel pathways through the anterior optic tubercle of the bumblebee (*Bombus ignitus*). J Comp Neurol 520:212–229.

Pfeiffer K, Kinoshita M, Homberg U. 2005. Polarization-sensitive and light-sensitive neurons in two parallel pathways passing through the anterior optic tubercle in the locust brain. J Neurophysiol 94:3903–3915.

Phillips-Portillo J. 2012. The central complex of the flesh fly, *Neobellieria bullata*: Recordings and morphologies of protocerebral inputs and small field neurons. J Comp Neurol 520:3088–3104.

Phillips-Portillo J, Strausfeld NJ. 2012. Representation of the brain's superior protocerebrum of the flesh fly, *Neobellieria bullata*, in the central body. J Comp Neurol 520:3070–3087.

Reppert SM, Gegear RJ, Merlin C. 2010. Navigational mechanisms of migrating monarch butterflies. Trends Neurosci 33:399–406.

Rind FC. 1987. Non-directional, movement sensitive neurones of the locust optic lobe. J Comp Physiol A 161:477–494.

Ritzmann RE, Ridgel AL, Pollack AJ. 2008. Multi-unit recording of antennal mechano-sensitive units in the central complex of the cockroach, *Blaberus discoidalis*. J Comp Physiol A 194:341–360.

Sakura M, Lambrinos D, Labhart T. 2008. Polarized skylight navigation in insects: model and electrophysiology of e-vector coding by neurons in the central complex. J Neurophys 99:667–682.

Sauman I, Briscoe AD, Zhu H, Shi D, Froy O, Stalleicken J, Yuan Q, Casselman A, Reppert SM. 2005. Connecting the navigational clock to sun compass input in monarch butterfly brain. Neuron 46:457–467.

Schildberger K. 1983. Local interneurons associated with the mushroom bodies and the central body in the brain of *Acheta domesticus*. Cell Tissue Res 230:573–586.

Schmitt S, Evers JF, Duch C, Scholz M, Obermayer K. 2004. New methods for the computer-assisted 3-D reconstruction of neurons from confocal image stacks. Neuroimage 23:1283–1298.

Siegl T, Schachtner J, Holstein GR, Homberg U. 2009. NO/cGMP signalling: L-citrulline and cGMP immunostaining in the central complex of the desert locust *Schistocerca gregaria*. Cell Tissue Res 337:327–340.

Strausfeld NJ. 1976. Atlas of an insect brain. New York: Springer.

Strausfeld NJ. 1999. A brain region in insects that supervises walking. Prog Brain Res 123:273–284.

Strausfeld NJ, Okamura J-Y. 2007. Visual system of calliphorid flies: organization of optic glomeruli and their lobula complex efferents. J Comp Neurol 500:166–188.

Strauss R. 2002. The central complex and the genetic dissection of locomotor behaviour. Curr Opin Neurobiol 12:633–638.

Träger U, Wagner R, Bausenwein B, Homberg U. 2008. A novel type of microglomerular synaptic complex in the polarization vision pathway of the locust brain. J Comp Neurol 506:288–300.

Triphan T, Poeck B, Neuser K, Strauss R. 2010. Visual targeting of motor actions in climbing *Drosophila*. Curr Biol 20: 663–668.

Vitzthum H, Homberg U. 1998. Immunocytochemical demonstration of locustatachykinin-related peptides in the central complex of the locust brain. J Comp Neurol 390:455–469.

Vitzthum H, M̈ller M, Homberg U. 2002. Neurons of the central complex of the locust *Schistocerca gregaria* are sensitive to polarized light. J Neurosci 22:1114–1125.

Wang Z, Pan Y, Li W, Jiang H, Chatzimanolis L, Chang J, Gong Z, Liu L. 2008. Visual pattern memory requires foraging function in the central complex of *Drosophila*. Learn Mem 15:133–142.

Wegerhoff R, Breidbach O, Lobemeier M. 1996. Development of locustatachykinin immunopositive neurons in the central complex of the beetle *Tenebrio molitor*. J Comp Neurol 375:157–166.

Wei H, el Jundi B, Homberg U, Stengl M. 2010. Implementation of pigment-dispersing factor-immunoreactive neurons in a standardized atlas of the brain of the cockroach *Leucophaea maderae*. J Comp Neurol 518:4113–4133.

Wendt B, Homberg U. 1992. Immunocytochemistry of dopamine in the brain of the locust *Schistocerca gregaria*. J Comp Neurol 321:387–403.

Williams JLD. 1975. Anatomical studies of the insect central nervous system: a ground-plan of the midbrain and an introduction to the central complex in the locust, *Schistocerca gregaria* (Orthoptera). J Zool 176:67–86.

Young JM, Armstrong J. 2010. Structure of the adult central complex in *Drosophila*: organization of distinct neuronal subsets. J Comp Neurol 518:1500–1524.

Zhu H, Sauman I, Yuan Q, Casselman A, Emery-Le M, Emery P, Reppert SM. 2008. Cryptochromes define a novel circadian clock mechanism in monarch butterflies that may underlie sun compass navigation. PLoS Biol 6:e4.